

Efficient suppression of premature termination codons with alanine by engineered chimeric pyrrolysine tRNAs

Aya Awawdeh¹, Alejandro Tapia^{2,3}, Sarah A. Alshawi⁴, Olabode Dawodu², Sarah A. Gaier⁵, Caitlin Specht², Jean-Denis Beaudoin⁴, Jeffery M. Tharp^{2,*} and Oscar Vargas-Rodriguez^{1,*,†}

¹Department of Molecular Biology and Biophysics, University of Connecticut School of Medicine, 263 Farmington Avenue, Farmington, CT 06030, USA

²Department of Biochemistry and Molecular Biology, Indiana University School of Medicine, 635 Barnhill Drive, Indianapolis, IN 46202, USA

³Department of Microbiology and Immunology, Indiana University School of Medicine, 635 Barnhill Drive, Indianapolis, IN 46202, USA

⁴Department of Genetics and Genome Sciences, Institute for Systems Genomics, University of Connecticut Health Center, 400 Farmington Avenue, Farmington, CT 06030, USA

⁵Barts and The London School of Medicine and Dentistry, Queen Mary University of London, 64 Turner Street, London, E1 2AD, UK

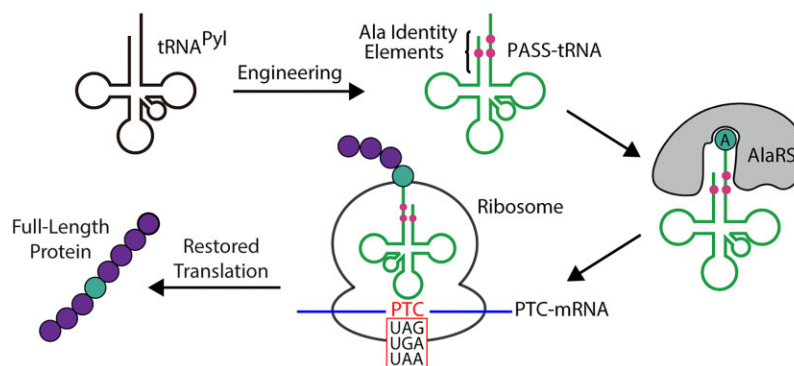
*To whom correspondence should be addressed. Tel: +1 860 679 8484; Email: vargasrodriguez@uchc.edu
Correspondence may also be addressed to Jeffery M. Tharp. Tel: +1 317 274 1520; Email: jemtharp@iu.edu

†The last two authors should be regarded as Joint Last Authors.

Abstract

Mutations that introduce premature termination codons (PTCs) within protein-coding genes are associated with incurable and severe genetic diseases. Many PTC-associated disorders are life-threatening and have no approved medical treatment options. Suppressor transfer RNAs (sup-tRNAs) with the capacity to translate PTCs represent a promising therapeutic strategy to treat these conditions; however, developing novel sup-tRNAs with high efficiency and specificity often requires extensive engineering and screening. Moreover, these efforts are not always successful at producing more efficient sup-tRNAs. Here we show that a pyrrolysine (Pyl) tRNA (tRNA^{Pyl}), which naturally translates the UAG stop codon, offers a favorable scaffold for developing sup-tRNAs that restore protein synthesis from PTC-containing genes. We created a series of rationally designed Pyl tRNA Scaffold Suppressor-tRNAs (PASS-tRNAs) that are substrates of bacterial and human alanyl-tRNA synthetase. Using a PTC-containing fluorescent reporter gene, PASS-tRNAs restore protein synthesis to wild-type levels in bacterial cells. In human cells, PASS-tRNAs display robust and consistent PTC suppression in multiple reporter genes, including pathogenic mutations in the tumor suppressor gene *BRCA1* associated with breast and ovarian cancer. Moreover, PTC suppression occurred with high codon specificity and no observed cellular dysregulation. Collectively, these results unveil a new class of sup-tRNAs with encouraging potential for tRNA-based therapeutic applications.

Graphical abstract



Introduction

More than 700 human diseases are caused by somatic and germline mutations that introduce premature termination codons (PTCs) into protein-coding genes (1). PTCs abort messenger RNA (mRNA) translation prematurely, producing

truncated proteins that can cause debilitating or fatal diseases. Currently, no treatment options are available for patients with most PTC-associated conditions. Thus, efforts to develop therapeutics are vital. One promising therapeutic strategy relies on engineered suppressor transfer RNAs (sup-tRNAs) (2–4).

Received: October 24, 2023. Editorial Decision: October 9, 2024. Accepted: October 21, 2024

© The Author(s) 2024. Published by Oxford University Press on behalf of Nucleic Acids Research.

This is an Open Access article distributed under the terms of the Creative Commons Attribution-NonCommercial License

(<https://creativecommons.org/licenses/by-nc/4.0/>), which permits non-commercial re-use, distribution, and reproduction in any medium, provided the original work is properly cited. For commercial re-use, please contact reprints@oup.com for reprints and translation rights for reprints. All other permissions can be obtained through our RightsLink service via the Permissions link on the article page on our site—for further information please contact journals.permissions@oup.com.

Recent studies have shown that engineered sup-tRNAs, delivered to cells using adeno-associated viral vectors or lipid nanoparticles, can promote translational PTC readthrough and rescue disease phenotypes in mouse models, thereby validating their therapeutic potential (5,6).

Previous efforts to engineer novel sup-tRNAs have primarily focused on changing the anticodon of canonical tRNAs that naturally recognize sense codons (6–9). However, the resulting anticodon-engineered sup-tRNA molecules often display low suppression activity. This is, in part, because natural tRNAs have evolved structural features to translate their cognate codons and cannot effectively compete with translation termination factors. Thus, additional mutations in other regions of the tRNA scaffold are generally required to improve the suppression activity of engineered sup-tRNAs (5,10,11). Although these mutations can significantly improve the efficiency of a sup-tRNA, the mechanistic details of how and why a given modification improves suppression activity are not always fully understood.

Naturally occurring sup-tRNAs, found in all domains of life (12), have evolved over billions of years to promote translational stop codon readthrough. In contrast to anticodon-engineered sup-tRNAs, naturally occurring sup-tRNAs have been refined by natural selection for PTC suppression. We hypothesized that repurposing naturally occurring sup-tRNAs for therapeutic applications might afford tRNA molecules with superior PTC suppression efficiency. To test this hypothesis, we focused on pyrrolysine (Pyl) tRNA (tRNA^{Pyl}), which is an efficient, naturally occurring sup-tRNA that installs Pyl, the 22nd proteinogenic amino acid (13). In nature, tRNA^{Pyl} is ligated with Pyl by pyrrolysyl-tRNA synthetase (PylRS). tRNA^{Pyl} delivers Pyl to the ribosome for its site-specific incorporation into proteins in response to in-frame UAG codons. The ability of tRNA^{Pyl} to translate stop codons has been exploited for synthetic biology applications, enabling the synthesis of proteins with over 200 non-canonical amino acids in diverse model organisms, including human cells and animal models (14–17). Thus, considering its natural suppression capacity and distinct structural features, tRNA^{Pyl} could offer a unique and versatile framework for developing sup-tRNA-based therapeutics.

A recent study showed that tRNA^{Pyl} , together with PylRS, can be used to restore dystrophin synthesis from a PTC-disrupted gene (18). This mutation is known to cause Duchenne muscular dystrophy, a disease characterized by progressive muscle weakness, and which is often fatal in the second or third decade of life (19). While this work underscored the therapeutic potential of tRNA^{Pyl} , the dependence on PylRS for tRNA aminoacylation complicates using this platform as a practical therapeutic strategy. Furthermore, this strategy requires co-administration of an unnatural amino acid substrate for PylRS. To overcome these limitations and fully harness the suppression capabilities of tRNA^{Pyl} for potential therapeutic applications, we sought to convert the tRNA into a substrate for a human aminoacyl-tRNA synthetase (aaRS), abrogating the need for co-delivery of PylRS and an unnatural amino acid. Herein, we describe the design and engineering of chimeric tRNA^{Pyl} molecules that are substrates of alanyl-tRNA synthetases (AlaRS). We demonstrate that these chimeric tRNAs can efficiently suppress diverse PTCs and rescue protein synthesis in *Escherichia coli* and cultured human cells. We show that these tRNAs retain the high suppression efficiency of tRNA^{Pyl} yet, because they are charged by an en-

dogenous aaRS, do not require simultaneous delivery of the PylRS gene or exogenous amino acids. Our results provide a new class of engineered sup-tRNAs and support the notion that natural sup-tRNAs offer a desirable scaffold for designing and developing novel sup-tRNAs.

Material and methods

General

Molecular cloning was performed using HiFi DNA Assembly (New England Biolabs) or In-Fusion Cloning (Takara) and *E. coli* Stellar cells (Takara). Synthetic oligonucleotides and gene fragments were purchased from Integrated DNA Technologies (IDT), the Keck Oligonucleotide Synthesis Facility at Yale University, and Sigma. DNA sequencing services were provided by GeneWiz, Quintarabio and the Keck DNA Sequencing Facility at Yale University. Mass spectrometry (MS) analysis of green fluorescent protein (GFP) expressed in HEK 293 was provided by the Indiana University School of Medicine Center for Proteome Analysis and, for GFP expressed in *E. coli*, by the University of Connecticut Proteomics and Metabolomics Facility. Nucleic acid sequences of tRNAs and protein reporters are listed in [Supplementary Tables S1](#) and [S2](#), respectively.

Plasmid construction

Plasmids expressing the wild-type (WT) *Methanomethylobacillus alvus* or *Methanosarcina mazei* Pyl tRNA and superfolder green fluorescent protein (sfGFP) (WT or with a termination codon at position 2) genes have been reported previously (20). The tRNAs are constitutively expressed under an *lpp* promoter, while sfGFP is controlled by an arabinose-inducible promoter. tRNA anticodon variants and sfGFP variants containing different stop codons were generated by site-directed mutagenesis. For experiments in HEK 293 cells, the WT *M. alvus* tRNA gene with an h7SK promoter was synthesized by IDT and cloned into an empty pBAD plasmid. To generate the tRNA variants, this template plasmid was modified by site-directed mutagenesis. To clone expression vectors with three copies of the tRNAs, h7SK-tRNA fragments were amplified with three primer sets having unique adapter sequences. The products of these PCRs were then simultaneously cloned into pCDNA3.1 recipient plasmids, encoding SEAP-40TAG (21) or GFP-150TAG (22), using NEBuilder[®] HiFi DNA Assembly. All plasmid constructs were confirmed by Sanger sequencing.

Fluorescence-based assay in *E. coli*

Escherichia coli BW25113 or MG1655 cells were transformed with pBAD plasmids encoding a PTC-containing sfGFP and one of the tRNA variants. Fresh colonies were used to inoculate 1 ml of Luria-Bertani (LB) media supplemented with ampicillin (100 $\mu\text{g}/\text{ml}$), and cells were grown overnight with continuous shaking at 37°C. 0.5 μl of the overnight culture was used to inoculate 99.5 μl LB media containing ampicillin (100 $\mu\text{g}/\text{ml}$) in the absence or presence of 0.15% arabinose in a 96-well black, clear-bottom plate. Cell density (OD_{600}) and sfGFP fluorescence intensity ($\lambda_{\text{ex}} = 485 \text{ nm}$, $\lambda_{\text{em}} = 510 \text{ nm}$) were monitored for 24 h with constant shaking at 37°C using a BioTek microplate reader (HTX or synergy H1). Data from the 24-h time point are reported. To remove the background signal, the fluorescence intensity values from uninduced cells were subtracted. Readthrough efficiency was calculated by

dividing sfGFP fluorescence by OD₆₀₀, and data were plotted using Prism 9 (GraphPad).

Purification and MS analysis of sfGFP from *E. coli*

Chemically competent *E. coli* MG1655 cells were transformed with a pBAD plasmid encoding either WT sfGFP with *M. alvus* tRNA^{V2.1}, sfGFP-S2TAG with tRNA^{V2.1} or sfGFP-S2TAG with tRNA^{V2.2}. Fresh colonies were used to inoculate 2 ml of LB media with ampicillin (100 µg/ml). Cells were grown overnight under continuous shaking at 37°C. The starter cultures were used to inoculate 50 ml of LB media with ampicillin, and the cell cultures were grown with continuous shaking at 37°C to an OD₆₀₀ of 0.7–1. sfGFP expression was induced with 0.2% arabinose overnight. The cultures were centrifuged at 6000 rpm for 15 min at 4°C. Cell pellets were resuspended with 750 µl lysis buffer [50 mM Tris (pH = 8), 300 mM NaCl, 10 mM imidazole and 1× BugBuster protein extraction reagent (Sigma)]. The lysed cells were centrifuged at 13 000 rpm for 35 min at 4°C, and the lysate was loaded on a column containing 0.6 ml TALON resin, pre-washed with 5 ml of deionized water and 3 ml of buffer containing 50 mM Tris (pH = 8), 150 mM NaCl and 10 mM imidazole. sfGFP was eluted using 1.5 ml of elution buffer [50 mM Tris (pH = 8), 300 mM NaCl and 300 mM imidazole]. Eluted protein was concentrated using a 10 kDa centrifugal filter unit (Millipore), and the proteins were stored in 50 mM Tris (pH = 8) and 150 mM NaCl. An aliquot containing 25 µg of purified sfGFP was diluted with 0.1 M ammonium bicarbonate (pH = 8), reduced at room temperature using 5 mM dithiothreitol for 1.5 h and then alkylated with 10 mM iodoacetamide for 45 min in the dark. Prior to the addition of protease, 100 mM CaCl₂ was added to yield a final concentration of 10 mM. Proteolysis was achieved using sequencing grade chymotrypsin (Promega Corporation P/N V1062) at an enzyme:protein ratio of 1:20 (*w/w*) and proceeded for 6 h at 37°C. The digestion was quenched using formic acid to yield a final pH of 2.5. Chymotryptic peptides were desalted using reversed-phase spin columns (Pierce™ P/N 89873) following the manufacturer's instructions. Desalted peptides were dried to completion, resuspended in 0.1% formic acid in water and quantified by measuring the absorbance at 280 nm on a NanoDrop spectrophotometer (Thermo Scientific). An aliquot containing 160 ng of peptides from each digestion was subjected to a 1 h reversed phase ultra-high performance liquid chromatography (UPLC) gradient using a Thermo Scientific Ultimate 3000 RSLCnano UPLC instrument. Peptides were eluted directly from the Waters nanoEase *m/z* Peptide BEH C18 analytical column (Waters Corporation P/N 186008795) into an Orbitrap Eclipse Tribrid mass spectrometer (Thermo Scientific) operated in positive electrospray mode using a 3 s maximum cycle time, TopN data-dependent acquisition method for tandem (MS/MS) acquisition. MS and MS/MS scans were acquired at high resolution in the Orbitrap mass analyzer. Peptide and protein identifications were generated by searching all raw UPLC-MS/MS raw files against the *E. coli* strain BL21(DE3) Uniprot annotated proteome database (identifier UP000002032, accessed 23 January 2023) plus a custom sfGFP database including WT sfGFP with all 20 standard amino acids in position 2, using the Andromeda search engine embedded in MaxQuant v1.6.10.43 (23). Variable modifications included oxidation of Met, acetylation of the protein N-terminus, deamidation of Asn/Gln and peptide N-terminal

Gln to pyro-Glu conversion. Carbamidomethylation of Cys was set as a fixed modification, and enzyme specificity was set to 'unspecific'. A 1% false discovery rate was used at the peptide-spectrum match (PSM), and protein levels and a minimum number of amino acids for an unspecific search were set to 6. All other parameters were left at default values. Search results were uploaded into Scaffold v5 (Proteome Software, Inc.) for data visualization and additional analysis. For label-free quantitative analysis of amino acids incorporated at residue 2, a 5 ppm mass window was used to generate extracted ion chromatograms in Xcalibur (Thermo Scientific) using theoretical monoisotopic masses for peptide sequences identified by MaxQuant. All charge states within the MS mass range were used for peak integrations. Stoichiometry estimates for residue 2 amino acids were not corrected to account for differences in ionization efficiency.

Cell culture

HEK 293 cells were purchased from ATCC (CRL-3216) and cultured in Dulbecco's modified Eagle medium with glutamine XL (Neta Scientific) supplemented with 10% fetal bovine serum (FBS; Gibco) and penicillin–streptomycin (Gibco). NCI-H1299 cells were purchased from ATCC (CRL-5803) and cultured in RPMI-1640 medium (ATCC) supplemented with 10% FBS (Gibco). All cell cultures were maintained in a humidified incubator at 37°C with a 5% CO₂ atmosphere.

Suppression assay with secreted embryonic alkaline phosphatase reporter in HEK 293

Cells were seeded in a 24-well plate and transfected with 0.5 µg of plasmid DNA using 3 µl FuGene6 (Promega) according to the manufacturer's protocol. Approximately 24 and 48 h after transfection, 25 µl of media was removed from each well, and the secreted embryonic alkaline phosphatase (SEAP) activity was quantified using the Phospha-Light™ SEAP Reporter Gene Assay System (Applied Biosystems) according to the manufacturer's protocol. Luminescence was measured in white, flat-bottom, 96-well plates using a BioTek Synergy H1 microplate reader (0.02 s/well). Data were normalized by dividing the luminescence signal of each sample by the signal of the positive control (SEAP with no PTC) and are displayed as the mean ± standard error of the mean (SEM) of three biological replicates.

Suppression assay with GFP reporter in HEK 293

For GFP quantification, cells were seeded in a six-well plate and transfected with 2 µg plasmid DNA using 12 µl FuGene6 (Promega) according to the manufacturer's protocol. Approximately 48 h after transfection, the media was removed and the cells were washed twice with PBS (Gibco). Cells were lysed for 20 min on ice using 150 µl of Radioimmunoprecipitation assay (RIPA) Lysis and Extraction Buffer (Thermo Scientific) supplemented with protease inhibitor cocktail (Thermo Scientific). Following lysis, the insoluble fraction was removed by centrifugation, and the supernatant was transferred to a new tube. Total protein content was measured using the Pierce™ BCA Protein Assay Kit according to the manufacturer's protocol. GFP fluorescence ($\lambda_{ex} = 485$ nm, $\lambda_{em} = 528$ nm) was quantified using 100 µl of cell lysate in black, clear-bottom 96-well plates in a BioTek Synergy H1 microplate reader. Relative GFP expression values were calculated by dividing the fluores-

cence signal by the total protein content for each sample, as described previously (22). Data were normalized by dividing each sample's relative GFP fluorescence by the positive control fluorescence (GFP with no PTC). Data are displayed as the mean \pm SEM of three biological replicates. For fluorescence imaging, cells were seeded in a 96-well plate and transfected with 0.1 μ g of plasmid DNA using polyethyleneimine (PEI) with a DNA:PEI ratio of 1:4. Cell images were collected ~48 h after transfection using an EVOS M5000 microscope.

Dual-luciferase assay

The dual-luciferase reporter plasmid containing the *Renilla* (Rluc) and firefly (Fluc) luciferase genes fused by a test sequence and tandem StopGo peptides was a gift from John Atkins (Addgene plasmid #119760; <http://n2t.net/addgene:119760>; RRID:Addgene_119760). A UAG PTC was inserted into the test sequence by site-directed mutagenesis. To measure sup-tRNA-mediated PTC suppression, NCI-H1299 cells were seeded in a white, clear-bottom 96-well plate and transfected with 100 ng of a pCDNA3.1 plasmid harboring the dual-luciferase reporter and sup-tRNA genes using FuGene6 (Promega). Rluc and Fluc activities were quantified 24 h after transfection using the Dual-Glo[®] Luciferase Assay kit (Promega), according to the manufacturer's protocol, in a Biotek Synergy H1 microplate reader.

Cell viability assay

The viability of HEK 293 cells expressing various sup-tRNAs was measured using the 3-(4,5-dimethylthiazol-2-yl)-2,5-diphenyltetrazolium bromide (MTT) assay (Cayman Chemical) according to the manufacturer's protocol. Briefly, ~20 000 viable cells (in 100 μ l of media) were seeded in each well of a 96-well plate. The following day, cells were transfected with the appropriate plasmids using FuGene6 (Promega) according to the manufacturer's protocol. Approximately 40 h after transfection, 10 μ l MTT reagent was added to each well, and the media was mixed. After an additional 3 h, 100 μ l of solubilization buffer was added, and each well was vigorously mixed. Absorbance at 570 nm was measured using a BioTek Synergy H1 microplate reader after incubating the plates for an additional 2 h at 37°C. Data are displayed as the mean \pm SEM of three biological replicates.

Enzyme purifications

Bacteriophage T7 RNA polymerase was purified as described previously (24). Human AlaRS was purified as described before with minor modifications (25). The pET21 plasmid encoding human AlaRS (a generous gift of Dr Xiang-Lei Yang, Scripps) was used to transform *E. coli* BL21(DE3). A single colony was used to inoculate 25 ml LB with ampicillin (100 μ g/ml). Cells were grown overnight at 37°C with continuous shaking. The seed culture was used to inoculate 1 L of LB supplemented with ampicillin. Cells were grown at 37°C with shaking to an OD₆₀₀ of 0.5. Protein overexpression was induced with 0.1 mM isopropyl β -D-1-thiogalactopyranoside (IPTG) for 16 h at 25°C. The cells were harvested by centrifugation, and the cell pellet was resuspended in buffer containing 50 mM Tris (pH = 8), 300 mM NaCl, 0.5 mM dithiothreitol and protease inhibitor tablets (Roche). Lysozyme (0.6 mg/ml) was added to the resuspension and incubated at 4°C for 30 min. The lysate was then sonicated for 15 min with 15 s-on and 45 s-off cycles on ice. The lysate was centrifuged at 4°C

for 45 min at 35 000 x g, and the soluble fraction was passed through a 0.45 μ m syringe filter; 2 ml of TALON resin was washed with water and equilibrated with wash buffer [50 mM Tris (pH = 8), 300 mM NaCl and 0.5 mM dithiothreitol]. The His-tagged protein was eluted with varying concentrations of imidazole. The protein was stored in 20 mM Tris (pH = 8), 200 mM NaCl, 1 mM dithiothreitol and 40% glycerol. For purification of *E. coli* AlaRS, the *E. coli* strain from the ASKA collection harboring the plasmid encoding *E. coli alaS* (26) was grown in LB media supplemented with chloramphenicol (34 μ g/ml). The culture was grown to an OD₆₀₀ of 0.6, and *E. coli* AlaRS overexpression was induced with 0.1 mM IPTG overnight at room temperature with shaking. Cells were collected by centrifugation, and the pellet was lysed with buffer containing 50 mM Tris (pH = 8), 300 mM NaCl and protease inhibitor tablets. The lysate was sonicated as described for human AlaRS. The lysate was centrifuged at 4°C for 75 min at 19 000 x g and then passed through a 0.45 μ m syringe filter; 2 ml of TALON resin was washed with water and equilibrated with wash buffer [50 mM Tris (pH = 8) and 300 mM NaCl]. The His-tagged protein was eluted with varying concentrations of imidazole solutions. The protein was stored in a buffer containing 50 mM HEPES (pH = 7.3), 150 mM NaCl and 40% glycerol. Protein concentrations were determined by the Bradford Assay.

tRNA transcript preparation

tRNAs were prepared using run-off *in vitro* transcription as previously described (27). Genes encoding PASS-tRNA^{V2.1}, PASS-tRNA^{V2.2} and PASS-tRNA^{V2.1.opal} were cloned downstream of the T7 promoter in a pUC18 plasmid. The DNA templates for PASS-tRNA^{V1.2}, PASS-tRNA^{V1.3}, WT *M. alvus* tRNA^{Pyl}, human WT tRNA^{Ala}, human tRNA^{Ala} with CUA anticodon, *E. coli* WT tRNA^{Ala} and *E. coli* WT tRNA^{Ala} with CUA anticodon with T7 promoter were ordered from Twist Bioscience. All tRNA DNA templates, together with the T7 promoter, were amplified via PCR for *in vitro* transcription reactions. 1 ml transcription reactions were carried out in 10 mM Tris-HCl (pH = 8), 20 mM MgCl₂, 1 mM spermidine; 0.01% Triton X-100, 5 μ g/ml bovine serum albumin (BSA), 4 mM NTPs, 8 μ g of DNA template, 5 mM dithiothreitol, 200 U/ml yeast pyrophosphatase and 0.235 mg/ml T7 RNA polymerase for 5 h at 37°C. The reaction was run on a 12% urea gel and tRNA transcripts were extracted with a solution of 1 mM ethylenediaminetetraacetic acid and 0.5 M ammonium acetate for 16 h at 37°C.

Aminoacylation assays

Aminoacylation reactions for human and *E. coli* AlaRS were carried out in 50 mM HEPES (pH = 7.3), 4 mM ATP, 10 mM MgCl₂, 0.1 mg/ml BSA, 1 mM DTT and 25 mM ¹⁴C-alanine with 0.25 μ M human or *E. coli* AlaRS and 5 μ M tRNA. tRNAs were refolded prior to the reaction by incubating at 80°C for 2 min, then at 60°C for 2 min, and adding 0.1 mM MgCl₂. The aminoacylation reaction was initiated by the addition of the enzymes and performed at 37°C. Time points (0 and 30 min) were taken by spotting 10 μ l of the reaction mixture on Whatman filter pads pre-soaked with 100 μ l of 5% trichloroacetic acid. The filter pads were washed with 5% trichloroacetic acid for 20 min three times and then washed with 100% ethanol. The filters were air-dried, and the bound ¹⁴C-alanine was measured in a liquid scintillation counter

(Beckman Coulter). All reactions were performed three times.

GFP MS

HEK 293 cells were seeded in a 60 mm dish and transfected with 5 µg of plasmid DNA using 30 µl of FuGene6 (Promega) according to the manufacturer's protocol. Approximately 48 h after transfection, the media was removed, and the cells were washed twice with PBS (Gibco) before being lysed on ice for 20 min using 0.5 ml RIPA Lysis and Extraction Buffer (Thermo Scientific) supplemented with protease inhibitor cocktail (Thermo Scientific). Following lysis, the insoluble fraction was removed by centrifugation, and the soluble lysate (500 µl) was diluted with 200 µl of dilution buffer [10 mM Tris (pH = 7.5), 150 mM NaCl and 0.5 mM ethylenediaminetetraacetic acid (EDTA)] supplemented with protease inhibitor cocktail tablets (Roche). The diluted lysate was mixed with 25 µl of ChromoTek GFP-Trap[®] Magnetic Agarose beads prewashed with dilution buffer. The beads-lysate mixture was incubated at 4°C for 1 h with end-over-end rotation. The protein-bound beads were washed three times with 0.5 ml wash buffer [10 mM Tris (pH = 7.5), 150 mM NaCl, 0.05% NP-40 and 0.5 mM EDTA] and once with dilution buffer. After the final wash, the beads were resuspended in 20 µl dilution buffer and stored at -80°C prior to MS.

For MS analysis, protein-bound beads were resuspended in 8 M urea and reduced with 5 mM TCEP at 35°C for 30 min. Following TCEP reduction, the sample was alkylated with 10 mM chloroacetylchloride for 30 min at room temperature. The alkylated sample was digested with 0.5 µg trypsin/LysC at 35°C overnight, and the digested sample was desalted using a C18 spin column. One half of the sample was injected using an EasyNano 1200 (Thermo Fisher Scientific) with a 25 cm EasySpray column (Cat. No. ES902, Thermo Fisher Scientific) and a 90 min LC gradient (hold at 8% B for 5 min, 8–35% B over 70 min, 35–80% B over 9 min, hold at 80% B for 1 min, 80–4% B over 5 min; Buffer A: 0.1% formic acid in water, Buffer B: 0.1% formic acid, 80% acetonitrile, 20% water). An Exploris 480 with FAIMS pro (Thermo Fisher Scientific) was used for the MS/MS analysis with field asymmetric waveform ion mobility spectrometry (FAIMS) compensation voltages (CVs) of -40, -55 and -70 V, each for 1.3 s cycle times. MS1 settings: orbitrap resolution of 120 000, RF lens 40%, standard automatic gain control (AGC) target, auto max IT, charge states of 2–7, dynamic exclusion 30 s. MS2 settings of 1.6 *m/z* isolation window, 30% Higher Energy Collision Dissociation, orbitrap resolution of 15 000, fixed first mass of 110 *m/z*, standard AGC target, and auto max IT. Data analysis was performed using PEAKS 11 (Bioinformatics Solutions) using the *Homo sapiens* Uniprot reference proteome (downloaded May 2022) supplemented with the GFP sequence and common laboratory contaminants. Following *de novo* peptide sequencing, a database search was performed with precursor mass tolerance of 10 ppm, fragment mass tolerance of 0.02 Da, semi-specific trypsin digest with a max of three missed cleavages, fixed modification of carbamidomethyl C and variable modifications of deamidation on N and Q and oxidation on M. Database search was followed by PEAKS PTM and PEAKS Spider searches to look for over 300 PTMs and any potential mutations. Data were filtered for a 1% PSM false discovery rate (FDR).

Ribosome profiling library preparation

HEK 293 cells were seeded in a 100 mm plate and transfected with 10 µg of an empty pCDNA3.1 plasmid (negative control) or a pCDNA3.1 plasmid containing three copies of tRNA^{V2.1} using FuGene6 (Promega). All samples were prepared in biological duplicate. 48 h after transfection, total RNA and ribosome-protected fragments (RPFs) were prepared as described previously (28) with a few modifications. Briefly, following digestion with RNase I, samples were placed on 1.4 ml of a sucrose cushion [1 M sucrose, 20 mM Tris (pH = 7.4), 150 mM NaCl, 5 mM MgCl₂, 100 µg/ml cycloheximide, 20 U/ml SUPERase•IN[™] RNase inhibitor] and centrifuged at 4°C for 2 h at 60 000 rpm. The supernatant was discarded and RPFs were purified from ribosome pellets using the miRNeasy Mini Kit (Qiagen). Size-selection of RPFs and total RNA by gel electrophoresis, dephosphorylation, linker ligation and subsequent purification were performed as described (29). Following purification, samples were pooled, and ribosomal RNA was depleted using the species-specific riboPOOL rRNA Depletion Kit (siTOOLS Biotech) according to manufacturer's protocol; 5' adapter ligation, cDNA synthesis and library amplification were performed as described previously (30). SuperScrip[™] IV Reverse Transcriptase (Invitrogen) was used for reverse transcription. NEBNext Multiplexed Oligos (NEB) and Phusion[™] High-Fidelity DNA Polymerase (Thermo Scientific) were used for library amplification. Following amplification, libraries were purified on an 8% TBE gel and sequenced by Azenta Life Sciences.

Ribosome profiling analysis

Paired-end sequencing (150 nt) was performed on an Illumina NovaSeq X Plus platform. Samtools was used to merge sequencing files for read 1 to produce one Fastq file per replicate. The Illumina TruSeq adapter sequence was trimmed from read 1 after aligning to the 3'-end, requiring a minimum global alignment score of 40 using ReadKnead v0.1.2 (doi.org/10.5281/zenodo.13948706). After trimming adapters, the unique molecular identifier (UMI) was trimmed from the 3' end and kept within the read name to identify PCR duplicates. Reads (only read 1) were aligned to the Ensembl 108 GRCh38 genome assembly using STAR v2.7.1a with the following non-default parameters: -alignEndsType EndToEnd, -sjdbScore 2, -outFilterMultimapNmax 1000, -outMultimapperOrder Random, -imitOutSAMoneReadBytes 600 000. SAM files produced were converted to BAM files with samtools. Duplicates were removed with rmdup v1.3. Profile counts were generated with GeneAbacus v0.2.2 (doi.org/10.5281/zenodo.13948696) with a minimum read overlap of 10 with transcript.

Ribosome Readthrough Scores (RRTS) were calculated as described previously (31). One transcript was selected per protein-coding gene. These transcripts were selected based on (i) complete coding sequences and UTRs, (ii) with the most 3' stop codon, and (iii) sequentially preferring primary APPRIS transcripts (32), (iv) inclusion in the consensus CDS gene set (33), and (v) those with the longest coding sequence. If more filtering of transcripts per gene was required, transcripts with the shortest 3'-UTR and then shortest 5'-UTR were selected. These transcripts were further filtered by those with

>200 reads in all samples. Ribosome footprint reads profiles were shifted by 13 nt to align the read start position to the ribosome P-site. The RRTS per transcript was calculated from the 3'-UTR ribosome density to the first termination codon in the 3'-UTR (3'TC) divided by the CDS ribosome density. The 3'-UTR ribosome density was calculated by summing the reads in the region 7nt after the CDS to the first 3'TC and dividing by the length of this region. Transcripts with <5 codons between the normal termination codon and the first 3'TC were discarded. CDS densities were calculated by reads per length of CDS, excluding the first 18 nts and last 15 nts.

RNA-sequencing analysis

Paired-end sequencing (150 nt) was performed on an Illumina NovaSeq X Plus platform. Samtools was used to merge sequencing files for read 1 to produce one Fastq file per replicate. The Illumina TruSeq adapter sequence was trimmed from read 1 after aligning to the 3' end, requiring a minimum global alignment score of 40 using ReadKnead v0.1.2 (doi.org/10.5281/zenodo.13948706). After trimming adapters, the UMI was trimmed from the 3' end and kept within the read name to identify PCR duplicates. Reads (only read 1) were aligned to the Ensembl 108 GRCh38 genome assembly using STAR v2.7.1a with the following non-default parameters: `-alignEndsType EndToEnd, -sjdbScore 2, -outFilterMultimapNmax 1000, -outMultimapperOrder Random, -imitOutSAMoneReadBytes 600 000`. SAM files produced were converted to BAM files with samtools v1.16.1. Duplicates were removed with rmdup v1.3. Counting was performed with GeneAbacus v0.2.2 (doi.org/10.5281/zenodo.13948696) with a minimum read overlap of 10 with transcript. Differential expression analysis was performed using DESeq2 v1.40.1 (34) with a parametric fit and custom R scripts.

UAG readthrough in *BRCA1*

For measuring PTC readthrough in *BRCA1*, we employed a fluorescence-based transactivation assay described previously (35,36). Briefly, the yeast Gal4 DNA-binding domain (Gal4; residues 1–100) was cloned from plasmid Gal4-VP16 (a gift from Lea Sistonen; Addgene plasmid # 71728; <http://n2t.net/addgene:71728>; RRID:Addgene_71728) as a genetic fusion to human *BRCA1* (residues 1396–1863) (a gift from Stephen Elledge; Addgene plasmid #14999; <http://n2t.net/addgene:14999>; RRID:Addgene_14999) in a pCDNA3.1 plasmid harboring three copies of the gene encoding tRNA^{V2.1} under control of a 7SK promoter. PTCs were then introduced into the *BRCA1* gene by site-directed mutagenesis. For measuring *BRCA1* activity, HEK 293 cells were seeded in a white, clear-bottom 96-well plate and co-transfected with the *Gal4-BRCA1* plasmid (22 ng), 5xGal4-TATA-luciferase (87 ng, a gift from Richard Maurer; Addgene Plasmid #46756; <http://n2t.net/addgene:46756>; RRID:Addgene_46756) and pLX313-*Renilla* (8.7 ng, a gift from William Hahn and David Root; Addgene plasmid #118016; <http://n2t.net/addgene:118016>; RRID:Addgene_118016) using LipofectamineTM 3000 according to the manufacturer's protocol. Fluc and Rluc activity were quantified 24 h after transfection using the Dual-Glo[®] Luciferase Assay Kit (Promega) in a BioTek Synergy H1 microplate reader.

Results

Rational design of Pyl tRNA Scaffold Sup-tRNAs

To develop a new class of human sup-tRNAs, we focused on tRNA^{Pyl}, a natural sup-tRNA found in a few bacterial and archaeal species (37). To harness the potential of tRNA^{Pyl}, we aimed to eliminate the requirements of co-expressing PylRS and the addition of exogenous amino acids by engineering the tRNA to be a substrate of an endogenous human aaRS (Figure 1A). We considered AlaRS an ideal candidate for three reasons. First, AlaRS's tRNA specificity is defined by five nucleotides in the acceptor stem (38,39). Therefore, in principle, only a few mutations are needed to convert tRNA^{Pyl} into a substrate of AlaRS (40). Notably, the anticodon is not a recognition element of AlaRS. Therefore, the anticodon of tRNA^{Pyl} may be mutated without impacting its recognition by AlaRS. Second, human and bacterial AlaRSs recognize the same tRNA elements (41), which enables facile screening of engineered tRNAs in *E. coli* for subsequent use in human cells. Third, the side chain of alanine consists of a small methyl group. Previous tRNAs developed for suppressing PTCs introduce amino acids with bulky or reactive side chains, such as tyrosine, arginine, or tryptophan (5,6,42). We surmise that the smaller side chain of alanine might minimize any disruptions to the structure and function of the protein encoded by PTC-containing genes. Based on this concept, we designed a series of tRNA^{Pyl} variants named Pyl tRNA Scaffold Sup-tRNAs (PASS-tRNAs).

Methanosarcina mazei-based PASS-tRNAs lack PTC suppression activity

Owing to its suppression efficiency and orthogonality, tRNA^{Pyl} from the archaeal species *M. mazei* is widely used in bacteria and human cells for genetic code expansion applications (13). Thus, we initially aimed to engineer *M. mazei* tRNA^{Pyl} into a substrate of AlaRS. First, we generated a series of *M. mazei* tRNA^{Pyl} mutants with different combinations of alanine tRNA identity elements in the acceptor stem. The resulting tRNA variants were named PASS-tRNA^{V1.1} (G73A), tRNA^{V1.2} (A3G/G73A) and tRNA^{V1.3} (A3G/A4G/U69C/G73A) (Supplementary Figure S1 and Supplementary Table S1). Next, the PTC suppression activity of the PASS-tRNAs was measured in *E. coli* using a fluorescence-based assay. In this assay, tRNAs are co-expressed with a sfGFP gene harboring an in-frame PTC (UAG) at position 2 (Figure 1B). Therefore, sfGFP is only produced if the PASS-tRNAs are aminoacylated by an *E. coli* aaRS and subsequently suppress the PTC. Unexpectedly, no sfGFP expression was detected in cells expressing any of the first-generation PASS-tRNAs (Supplementary Figure S1), suggesting that the *M. mazei*-based tRNAs were either not aminoacylated by *E. coli* aaRSs or could not suppress the PTC in sfGFP. In contrast, an *E. coli* tRNA^{Ala} mutant carrying a CUA anticodon promoted sfGFP expression with a suppression efficiency of 13.6% relative to WT sfGFP (Supplementary Figure S1).

Methanomethylophilus alvus tRNA^{Pyl}-based PASS-tRNAs efficiently suppress PTCs with alanine

Because the *M. mazei* tRNA^{Pyl} mutants could not suppress UAG PTCs, we changed our focus to a tRNA^{Pyl} from a

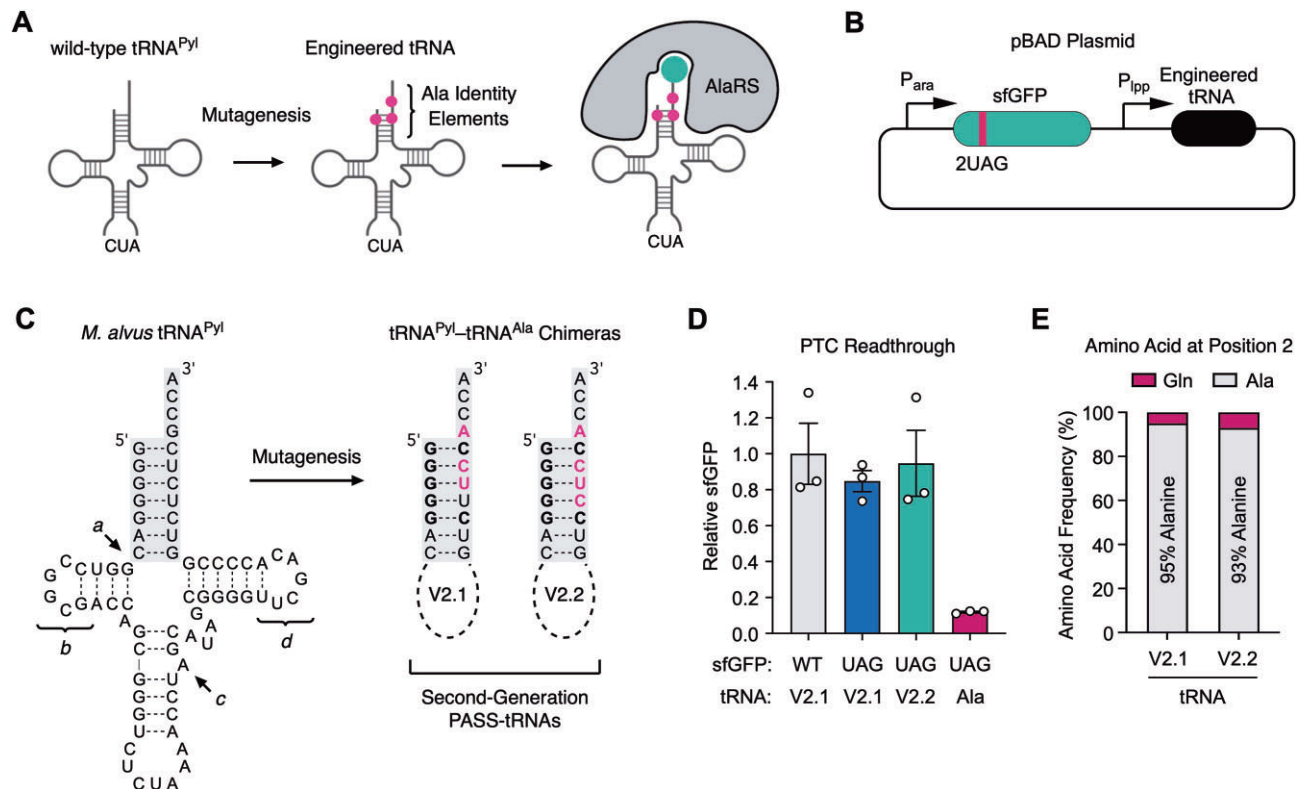


Figure 1. (A) Rational design of suppressor tRNAs for PTC translation. The alanine identity elements were introduced into the acceptor stem of the Pyl tRNA ($tRNA^{Pyl}$) to generate PASS-tRNAs. The resulting tRNAs were expected to be charged with alanine by the human and *E. coli* AlaRS. (B) Schematic representation of the plasmid used to measure PTC suppression efficiency of our engineered chimeric tRNAs in bacterial cells. PTC suppression was quantified using a sfGFP reporter gene containing a UAG stop codon at position 2. sfGFP synthesis only occurs if our engineered tRNAs suppress the PTC. (C) The structure of $tRNA^{Pyl}$ from *M. alvus* and the acceptor stems of two second-generation PASS-tRNAs (V2.1 and V2.2). Unique features of the *M. alvus* $tRNA^{Pyl}$ are indicated: (a) a missing base between the acceptor and D stem, (b) minimal D loop, (c) an unpaired base in the anticodon stem, and (d) a shortened T loop. Mutations introduced into the *M. alvus* $tRNA^{Pyl}$ to generate PASS-tRNAs V2.1 and V2.2 are shown in magenta. Nucleotides in the engineered tRNAs that are also present in the human alanine tRNA are shown in bold. (D) sfGFP expression in cells expressing a WT sfGFP gene (WT), a sfGFP gene with a PTC at position 2 (UAG) and one of the engineered PASS-tRNAs (V2.1 or V2.2), or a sfGFP gene with a PTC at position 2 and an anticodon-engineered *E. coli* alanine tRNA (Ala). Data are presented as the mean \pm SEM of three biological replicates. (E) Amino acid incorporation at the PTC-encoded position (position 2) of sfGFP as determined by MS.

distantly related archaeal species, namely *Methanomethylophilus alvus*. *M. alvus* $tRNA^{Pyl}$ has several unique structural features not found in the *M. mazei* $tRNA^{Pyl}$, including the lack of a base at the intersection of the acceptor and D arms, shortened D and T loops and a bulge in the anticodon stem (13,43) (Figure 1C). Previous studies showed that the *M. alvus* $tRNA^{Pyl}$ is active and orthogonal in *E. coli* and human cells (22,44,45), and recent data suggest that the *M. alvus* $tRNA^{Pyl}$ suppresses UAG codons more efficiently than *M. mazei* $tRNA^{Pyl}$ (37). We created two second-generation PASS-tRNAs, $tRNA^{V2.1}$ (C70U/U71C/G73A) and $tRNA^{V2.2}$ (U69C/C70U/U71C/G73A), by transplanting alanine identity elements into the acceptor stem of *M. alvus* $tRNA^{Pyl}$ (Figure 1C and Supplementary Table S1). We then measured PTC suppression with $tRNA^{V2.1}$ and $tRNA^{V2.2}$ in *E. coli* using our fluorescence-based assay. The expression of $tRNA^{V2.1}$ and $tRNA^{V2.2}$ resulted in efficient UAG suppression, restoring sfGFP synthesis to WT levels (sfGFP with no PTC) (Figure 1D). In contrast, the *E. coli* $tRNA^{Ala}$ variant with a CUA anticodon showed weak suppression activity (Figure 1D), highlighting the enhanced PTC translation activity afforded by the *M. alvus* $tRNA^{Pyl}$ scaffold.

To determine the identity of the amino acid(s) inserted in response to the PTC, we purified sfGFP from cells co-

expressing $tRNA^{V2.1}$ or $tRNA^{V2.2}$ and subsequently analyzed the proteins by tandem MS. The analysis revealed that 95% of the sfGFP co-expressed with $tRNA^{V2.1}$ and 93% of sfGFP co-expressed with $tRNA^{V2.2}$ contained alanine at the PTC-encoded position (Figure 1E and Supplementary Figure S2). These data confirm our hypothesis that the *E. coli* AlaRS recognizes $tRNA^{V2.1}$ and $tRNA^{V2.2}$ *in vivo*. Approximately 5–7% of sfGFP contained glutamine incorporated in response to the PTC. Glutamine at the PTC-encoded position is likely a result of misincorporation at UAG codons due to near-cognate suppression by endogenous $tRNA^{Gln}$, as observed previously (46,47).

Aminoacylation is not a limiting factor for PTC suppression by PASS-tRNAs

Intrigued by the contrasting suppression activity of *M. mazei* and *M. alvus* tRNA variants, we decided to test whether tRNA aminoacylation by AlaRS is a determining factor in PTC decoding. To this end, we performed *in vitro* aminoacylation assays using tRNA transcripts and purified recombinant *E. coli* AlaRS. The results showed varying aminoacylation efficiencies for the PASS-tRNA variants relative to WT *E. coli* $tRNA^{Ala}$ (Figure 2A); however, aminoacylation efficiency did not corre-

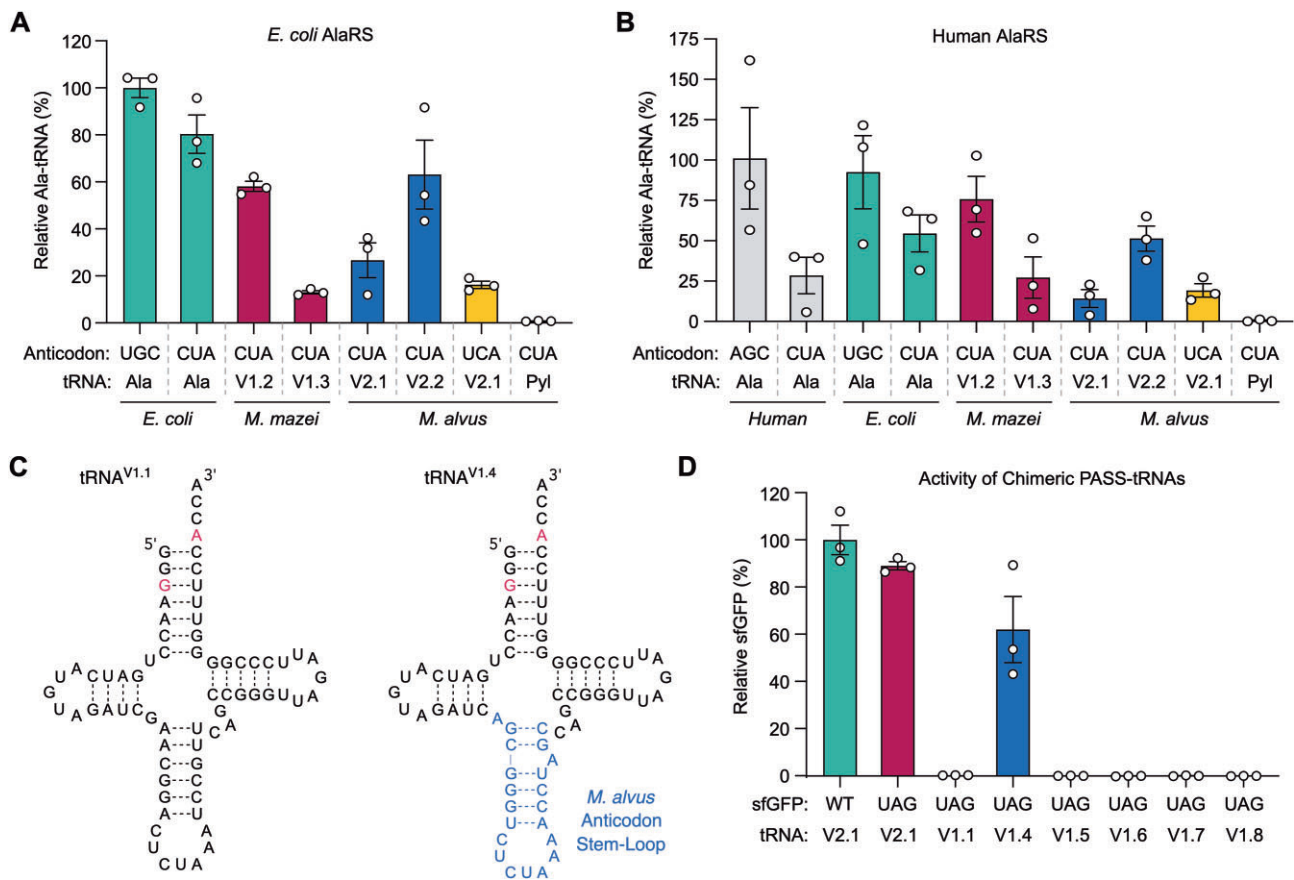


Figure 2. (A, B) *In vitro* aminoacylation of engineered and WT tRNAs with alanine by *E. coli* (A) and human (B) AlaRS. Data are presented as the mean \pm SEM of three replicate experiments. (C) The secondary structures of *M. mazei*-based PASS-tRNAs V1.1 and V1.4. PASS-tRNA^{V1.4} is a chimera harboring the *M. alvus* anticodon stem-loop. (D) sfGFP expression in *E. coli* cells expressing a WT sfGFP gene (WT) or a sfGFP gene with a PTC at position 2 (UAG) and one of the engineered PASS-tRNAs. Data are presented as the mean \pm SEM of three biological replicates.

late with PTC readthrough efficiency. For example, tRNA^{V1.2}, which showed no PTC translation in the sfGFP assay, was aminoacylated with similar efficiency as the strong PTC suppressor tRNA^{V2.2}. As expected, the WT *M. alvus* tRNA^{Pyl} lacking alanine identity elements was not aminoacylated by AlaRS. The data also revealed that the anticodon alteration of *E. coli* tRNA^{Ala} minimally affects aminoacylation. Together, these results demonstrate that differences in aminoacylation efficiency do not explain the difference in PTC suppression by *M. mazei* and *M. alvus*-based PASS-tRNAs.

Because PASS-tRNAs are intended for use in human cells, we also performed *in vitro* aminoacylation assays using human cytosolic AlaRS. Similar levels of aminoacylation for WT human and *E. coli* tRNA^{Ala} were observed, but these tRNAs were aminoacylated less efficiently when the anticodon was changed to CUA (Figure 2B). Notably, the relative aminoacylation of PASS-tRNA variants by human and *E. coli* AlaRS enzymes was similar (compare Figure 2A and B). These results validate our approach for developing a human alanine sup-tRNA in *E. coli*, as the bacterial and human AlaRS enzymes use a similar mechanism of tRNA substrate selection.

The anticodon stem-loop of *M. alvus* tRNA^{Pyl} is a key feature for PTC translation

Given that the aminoacylation efficiency of AlaRS does not appear to limit PTC translation by PASS-tRNAs, we surmised

that structural features in the *M. alvus* tRNA^{Pyl} may be responsible for its ability to translate PTCs more efficiently than *M. mazei* PASS-tRNAs. To test this hypothesis, we created a series of chimeric PASS-tRNAs (V1.4–V1.8) by transplanting stem-loop branches from the *M. alvus* tRNA^{Pyl} onto the *M. mazei* tRNA^{Pyl} scaffold (Supplementary Figure S3 and Supplementary Table S1). The PTC suppression efficiency of the resulting tRNA chimeras was tested using our sfGFP reporter in *E. coli* (Figure 1B). Interestingly, only one of the chimeric tRNAs, PASS-tRNA^{V1.4}, facilitated PTC suppression and restored robust sfGFP synthesis (Figure 2C, and D). This tRNA carries the anticodon stem-loop of the *M. alvus* tRNA^{Pyl}, suggesting that this structural feature is essential for the translation efficiency of *M. alvus* PASS-tRNAs.

PASS-tRNAs efficiently rescue premature UAG codons in human cells

Based on their robust suppression efficiency in *E. coli*, we next tested the *M. alvus* PASS-tRNAs in human cells. To monitor PTC suppression, we generated plasmids encoding three copies of a PASS-tRNA gene (tRNA^{V2.1} or tRNA^{V2.2}) and a GFP reporter gene containing a PTC (UAG) at position 150 (Figure 3A). We transiently transfected HEK 293 cells with these plasmids and measured the resulting GFP expression. Under these conditions, GFP is only produced if the PASS-tRNAs suppress the PTC in the GFP gene. Fluor-

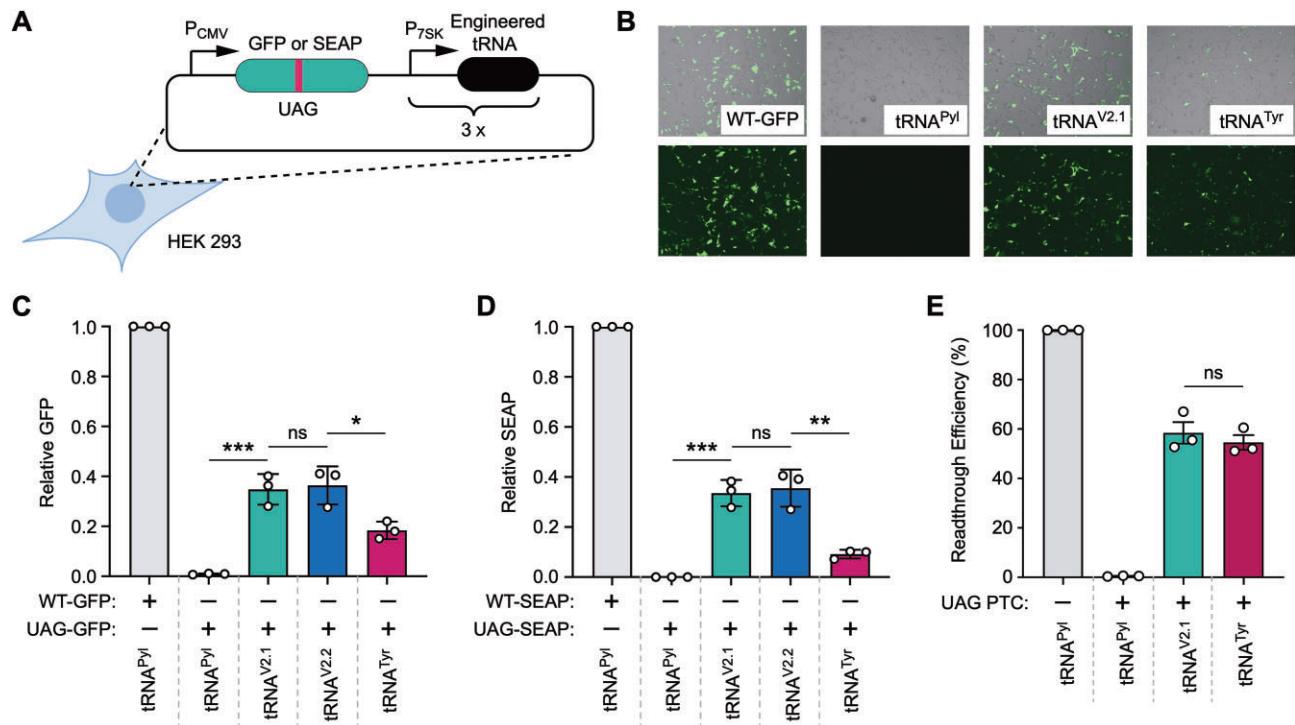


Figure 3. (A) A map of the plasmid used to measure PTC suppression in HEK 293 cells. The plasmid contains three copies of the indicated tRNA and either a GFP reporter gene harboring a UAG PTC at position 150 or a SEAP reporter gene carrying a UAG PTC at position 40. (B) Fluorescence images of cells expressing the WT GFP gene (WT-GFP) and the WT tRNA^{Pyl}, or a GFP gene harboring a PTC at position 150 and WT tRNA^{Pyl}, an engineered PASS-tRNA (tRNA^{V2.1}), or an anticodon-engineered human tyrosine tRNA (tRNA^{Tyr}). (C) Relative GFP expression in cells expressing the WT GFP reporter (WT-GFP) or the GFP reporter with a UAG PTC at position 150 (UAG-GFP) and the indicated tRNA. (D) SEAP expression in cells expressing a WT SEAP reporter gene (WT-SEAP) or a SEAP reporter harboring a UAG PTC at position 40 (UAG-SEAP) and the indicated tRNA. (E) UAG readthrough efficiency of the indicated sup-tRNA as measured using a dual-luciferase reporter with a PTC-containing test sequence. Data are the mean \pm SEM of three biological replicates. (* $P < 0.05$, ** $P < 0.005$, etc.; ns, not significant; paired t -test).

rescence imaging of cells expressing tRNA^{V2.1} showed GFP expression, whereas the WT *M. alvus* tRNA^{Pyl} did not (Figure 3B), underscoring the requirement of alanine identity elements for aminoacylation. Quantification of GFP fluorescence revealed that tRNA^{V2.1} and tRNA^{V2.2} restored GFP levels to $\sim 35\%$ relative to WT GFP (no PTC) (Figure 3C). To confirm that the PTC-encoded position was translated as alanine in HEK 293 cells, we purified GFP co-expressed with tRNA^{V2.1} and analyzed the protein using tandem MS. In this analysis, 22 unique peptides corresponding to GFP were identified. Three of the GFP-derived peptides included the PTC-encoded position, and all three peptides displayed mass and fragmentation patterns consistent with alanine incorporation (Supplementary Figure S4). This observation further supports the conclusion that tRNA^{V2.1} is a substrate for human AlaRS *in vivo*.

To further examine the suppression capacity of PASS-tRNAs in human cells, we employed a second reporter based on the secreted embryonic alkaline phosphatase (SEAP) gene containing a PTC (UAG) at position 40. Suppression of the PTC by PASS-tRNAs leads to the synthesis of SEAP, which is secreted into the media and can be measured using commercially available substrates (21,48). Consistent with the GFP-based assay, tRNA^{V2.1} and tRNA^{V2.2}, but not WT tRNA^{Pyl}, displayed robust suppression efficiency. With both PASS-tRNAs, SEAP production levels were restored to $\sim 34\%$ of WT (Figure 3D). The SEAP expression level continued to increase, relative to the WT gene, for all sup-tRNAs tested from 24 to 48 h after transfection (Supplementary Figure S5). Interestingly, the suppression efficiency of PASS-tRNAs is com-

parable in both GFP and SEAP reporters (Figure 3C and D), suggesting that the engineered tRNAs can translate UAG codons with similar efficiency in two different mRNA coding contexts.

PASS-tRNA's translation efficiency relative to anticodon-engineered human sup-tRNAs

Recent efforts to create sup-tRNAs have focused on altering the anticodon of canonical human tRNAs (5,6,9,42). For example, a human tRNA^{Tyr} with a single anticodon mutation (G34C) was shown to rescue a UAG PTC in cultured cells and a mouse model of a human disease (6). To compare the suppression efficiency of PASS-tRNAs and the anticodon mutant of the human tyrosine tRNA (sup-tRNA^{Tyr}), we measured UAG readthrough using both the SEAP and GFP assays. Notably, PASS-tRNAs displayed higher suppression efficiency relative to sup-tRNA^{Tyr} in both reporters. Both PASS-tRNA variants were almost 2- and 4-fold more efficient than sup-tRNA^{Tyr} in the GFP and SEAP reporters, respectively (Figure 3B–D).

The experiments using SEAP and GFP reporter genes suggest that PASS-tRNAs suppress PTCs more efficiently than sup-tRNA^{Tyr}; however, these assays rely on fluorescence and luminescence measurements that could be influenced by the identity of the amino acid installed at the PTC-encoded position. Since PASS-tRNAs and sup-tRNA^{Tyr} install alanine and tyrosine, respectively, these reporters may not accurately reflect suppression efficiency of the sup-tRNAs and may instead reflect the difference in fluorescence and luminescence

with alanine versus tyrosine installed at the PTC-encoded position. To obtain a more accurate measure of suppression efficiency, we employed a previously developed dual-luciferase reporter specifically designed to mitigate the effect of different amino acids at the target position (49). This reporter is a fusion protein composed of the *Renilla* (Rluc) and Firefly (Fluc) luciferase coding sequences linked by a PTC-containing test sequence (Supplementary Figure S6). Tandem StopGo peptides upstream and downstream of the test sequence cotranslationally cleave the Rluc, Fluc and test sequence into distinct polypeptides, thereby ensuring that the same Rluc and Fluc reporter proteins are produced irrespective of the amino acid composition of the test sequence. To measure sup-tRNA-mediated suppression, we transiently transfected NCI-H1299 cells with a plasmid harboring the dual-luciferase reporter, with a UAG PTC in the test sequence, and three copies of the genes encoding tRNA^{V2.1}, WT tRNA^{Pyl} or sup-tRNA^{Tyr} and quantified Rluc and Fluc activities after 24 h. tRNA^{V2.1} displayed slightly higher suppression than sup-tRNA^{Tyr}; however, the difference was not statistically significant (Figure 3E).

We also created a human tRNA^{Ala} with a suppressor anticodon to test whether the mutant tRNA can translate the UAG stop codon (Figure 4A). Like the *E. coli* tRNA^{Ala}, the anticodon-engineered human tRNA^{Ala} showed very weak UAG suppression, restoring <1% of WT SEAP expression (Figure 4B).

PASS-tRNA expression does not reduce cell viability

We surmised that the expression of highly efficient sup-tRNAs may be toxic to cells due to potential readthrough of native termination codons. Therefore, we used the MTT assay to assess cell viability upon sup-tRNA expression. HEK 293 cells expressing either tRNA^{V2.1}, tRNA^{V2.2}, or the anticodon-engineered human sup-tRNA^{Tyr} showed no significant decrease in viability compared to cells expressing WT tRNA^{Pyl} over 48 h (Supplementary Figure S7). To further investigate potential undesired effects of PASS-tRNAs, we performed a comparative transcriptomic analysis using total mRNA from HEK 293 cells harboring an empty vector or a vector expressing tRNA^{V2.1}. We found that expressing PASS-tRNA^{V2.1} in HEK 293 cells does not elicit significant changes in the cellular transcriptome (Supplementary Figure S7), suggesting that the tRNA does not interfere with transcriptional homeostasis or detectably trigger off-target pathways. The only significantly upregulated gene in PASS-tRNA-expressing cells relative to control cells was *HMOX1*, encoding Heme Oxygenase 1, an enzyme involved in iron metabolism (50). Further studies are required to better understand the mechanistic rationale for *HMOX1* upregulation and its potential biological significance. However, the cell viability and gene expression data collectively support recent studies demonstrating low toxicity and off-target activity of sup-tRNAs in human cells (5,6).

PASS-tRNA^{V2.1} does not promote transcriptome-wide suppression of native termination codons

A key safety consideration with respect to the therapeutic use of sup-tRNAs is their potential for translating natural termination codons. Off-target translation of native stop codons would cause the synthesis of proteins with extended C-termini that could dysregulate the proteome. To determine the extent

to which PASS-tRNAs disrupt translation termination of native genes, we used ribosome profiling to quantify global stop codon readthrough in HEK 293 cells transfected with a plasmid expressing tRNA^{V2.1} and compared the level of stop codon readthrough to cells transfected with an empty vector. Our calculated RRTS, which measure the density of ribosomes in the 3'-UTR (31), show only a minor increase in readthrough of native stop codons relative to control cells not expressing tRNA^{V2.1} (RRTS = 0.07 and 0.09 for control and treated cells, respectively; Figure 4C). These results indicate that tRNA^{V2.1} does not greatly increase readthrough of native termination codons, in agreement with several recent studies showing minimal native stop codon readthrough elicited by sup-tRNAs (5,6,9).

Codon specificity and plasticity of PASS-tRNAs

Near-cognate stop codon readthrough has been observed for sup-tRNAs (20,51,52), which can have undesirable side effects. To evaluate whether PASS-tRNAs have off-target decoding activity, we tested the ability of PASS-tRNA^{V2.1} to decode near-cognate stop codons. This was achieved by measuring sfGFP expression in cells co-expressing PASS-tRNA^{V2.1} and a sfGFP mutant gene with UAA or UGA PTC at position 2 (Figure 5A). Notably, co-expression of PASS-tRNA^{V2.1} with the sfGFP reporters containing UAA and UGA codons in *E. coli* cells did not yield sfGFP synthesis (Figure 5B). These results demonstrate that PASS-tRNAs translate the UAG stop codon with high specificity. Next, we asked whether PASS-tRNAs can be modified to promote translational readthrough of PTCs other than UAG. To probe whether PASS-tRNAs can translate the UAA and UGA nonsense codons, we changed the anticodon of tRNA^{V2.1} to UUA or UCA, respectively. We then expressed these anticodon mutants in HEK 293 cells co-expressing the SEAP reporter gene with a corresponding PTC at position 40 (Figure 5C). While PTC readthrough was most efficient with UAG, the PASS-tRNA mutants also afforded readthrough of both UAA and UGA. The PASS-tRNA mutant bearing a UUA anticodon restored GFP expression to ~6% of WT GFP, while the PASS-tRNA mutant harboring a UCA anticodon restored GFP expression to >15% that of the WT gene (Figure 5D). As expected, WT tRNA^{Pyl}, bearing the corresponding anticodon mutations, did not suppress either UGA or UAA PTCs in HEK 293 since this tRNA is not aminoacylated by any human aaRS (Figure 5D).

For comparison, we also tested UGA and UAA PTC suppression using anticodon mutants of the human tyrosine tRNA. While mutant sup-tRNA^{Tyr} suppressed both UGA and UAA, the suppression efficiency was low (Figure 5D). Indeed, anticodon mutants of PASS-tRNA^{V2.1} suppressed UGA and UAA PTCs 86- and 4.6-fold more efficiently than sup-tRNA^{Tyr} mutants, respectively. The poor suppression capabilities of tRNA^{Tyr} anticodon mutants likely result from decreased aminoacylation efficiency since the anticodon is a recognition element for TyrRS (53). Collectively, these data demonstrate that PASS-tRNAs may be used to target PTC-related diseases involving any of the three nonsense codons in human cells.

PASS-tRNAs suppress pathogenic PTCs in *BRCA1*

Finally, we asked whether PASS-tRNAs could suppress pathogenic PTCs to restore synthesis of functional proteins. We selected the tumor suppressor gene *BRCA1* as a model

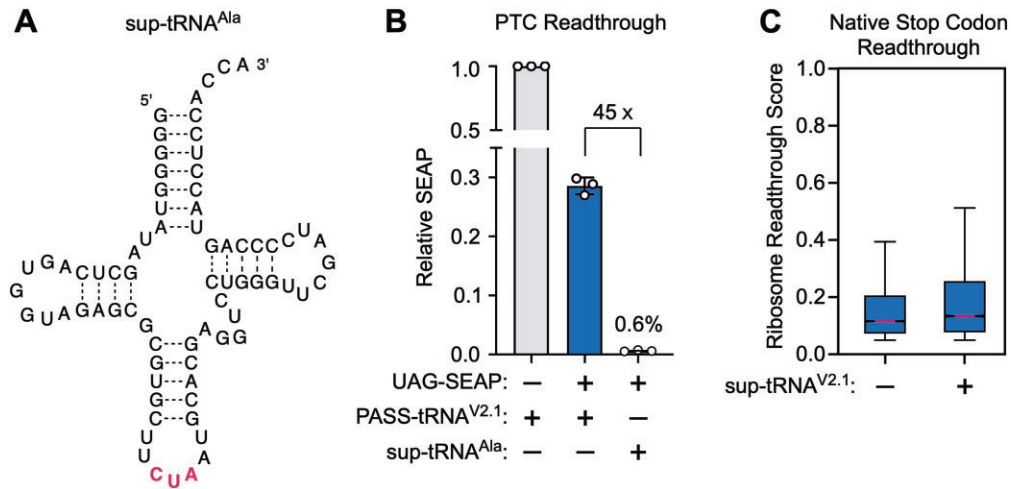


Figure 4. (A) The predicted cloverleaf structure of anticodon-engineered human alanine tRNA (sup-tRNA^{Ala}). (B) PTC readthrough in HEK 293 cells co-expressing WT SEAP and PASS-tRNA^{V2.1} or SEAP with a UAG PTC at position 40 and either PASS-tRNA^{V2.1} or sup-tRNA^{Ala}. Data are displayed as the mean \pm SEM of three biological replicates. (C) Ribosome readthrough scores determined for HEK 293 cells transfected with an empty vector (-) or a vector harboring three copies of PASS-tRNA^{V2.1} (+). Data are pooled from two biological replicates. The median is displayed in magenta. Box edges represent first and third quartiles. Whiskers represent 1.5 times the interquartile range.

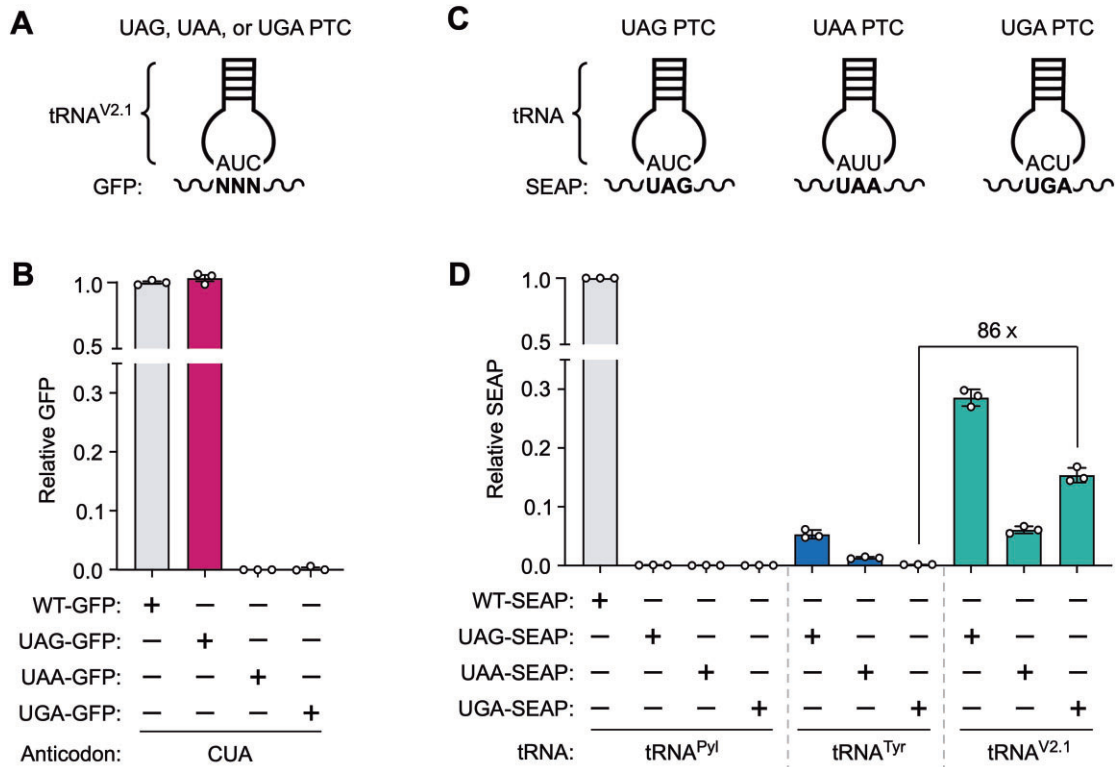


Figure 5. (A) To test the PTC specificity of PASS-tRNA^{V2.1}, position 2 of sfGFP was changed to either of the three termination codons (UAG, UAA, and UGA). (B) sfGFP expression in *E. coli* cells co-expressing either WT or PTC-containing sfGFP and sup-tRNA^{V2.1}. (C) The versatility of PASS-tRNAs to suppress PTCs caused by UAG, UAA and UGA mutations was tested by swapping the anticodon of sup-tRNA^{V2.1} to CUA, UUA or ACU to match the target PTC. (D) SEAP expression in HEK 293 cells was measured for a WT SEAP (WT-SEAP) or a SEAP reporter gene harboring a UAG, UAA or UGA PTC at position 40 (UAG-SEAP, UAA-SEAP and UGA-SEAP, respectively). SEAP expression was measured in cells co-expressing anticodon mutants of the WT tRNA^{Pyl}, anticodon-engineered human tyrosine tRNA (tRNA^{Tyr}), or tRNA^{V2.1}.

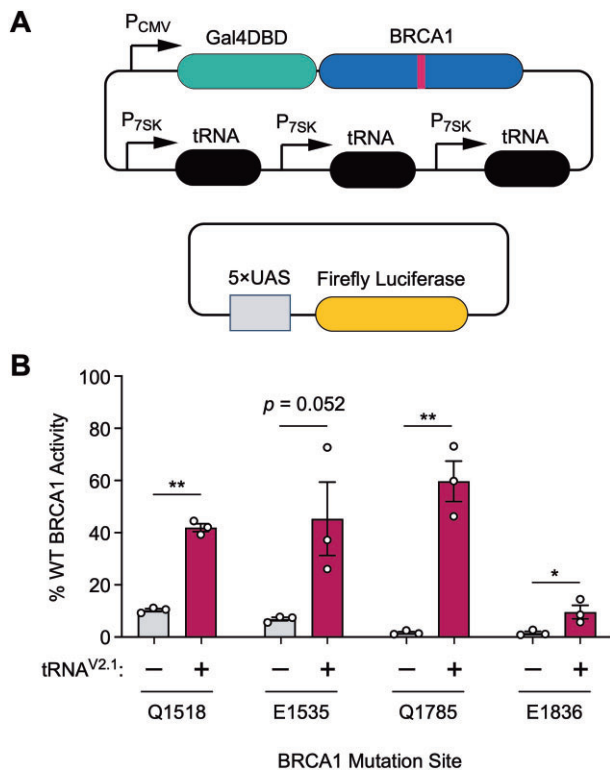


Figure 6. (A) Schematic representation of the plasmid system used to measure PTC suppression in *BRCA1*. Human *BRCA1* (residues 1396–1863) containing an in-frame UAG PTC was expressed as a genetic fusion to the Gal4 DNA-binding domain (Gal4DBD). Three copies of tRNA^{V2.1} were expressed from the same plasmid. The Gal4DBD-*BRCA1* plasmid was co-transfected with a plasmid containing the firefly luciferase (*Fluc*) gene and five copies of the Gal4 upstream activation sequence (5× UAS). In this assay, *Fluc* transcription is dependent on *BRCA1*-mediated transactivation. (B) *BRCA1* activity in HEK 293 cells expressing *BRCA1* with a UAG PTC at the indicated position with (+) and without (-) co-expression of tRNA^{V2.1}. Data are displayed as the mean ± SEM of three biological replicates. **P* < 0.05, ***P* < 0.005, unpaired student's *t*-test.

since nonsense mutations within *BRCA1* significantly increase the risk of developing several types of cancer, principally breast and ovarian cancer (54). We measured suppression by tRNA^{V2.1} of four clinically relevant PTCs occurring at codons Q1518, E1535, Q1785 and E1836. These mutations were chosen, in part, because they were previously shown to tolerate amino acid substitutions without substantially impacting *BRCA1* activity (35). We utilized a previously reported assay for measuring *BRCA1*-mediated transactivation of a luciferase reporter gene in HEK 293 cells with and without co-expression of tRNA^{V2.1} (Figure 6A) and compared the activity to that of WT *BRCA1* (without a PTC). With each nonsense variant, cells expressing tRNA^{V2.1} displayed higher *BRCA1* activity than cells not expressing a sup-tRNA (Figure 6B); however, the level of *BRCA1* activity varied. For the Q1518, E1535 and Q1785 mutants, *BRCA1* activity was restored to between 42 and 60% of that of cells expressing WT *BRCA1*, whereas with the E1836 mutant, *BRCA1* activity was restored to <10% of WT. This discrepancy may be due to differences in suppression efficiency of PTCs in different sequence contexts. The background activity of each of the PTC mutants also varied significantly, suggesting that sequence context contributes to background suppression. An alternative explanation is that

the E1836 variant does not tolerate alanine substitution as well as the other mutants. Nonetheless, these data demonstrate that tRNA^{V2.1} can suppress pathogenic PTCs within *BRCA1* to restore functional *BRCA1* protein.

Discussion

In this work, we developed sup-tRNAs by combining the framework of tRNA^{Pyl}, a naturally occurring and efficient sup-tRNA, with the identity elements of tRNA^{Ala}. The resulting engineered tRNAs showed robust suppression efficiency in bacterial and human cells. The facile development of PASS-tRNAs using *E. coli* as an engineering platform provides a proof of concept that may be expanded to improve PASS-tRNAs or potentially devise new tRNA^{Pyl}-inspired sup-tRNAs with different amino acid identities. This could be achieved by integrating rational design (55,56) and directed evolution approaches (57,58) to change the identity of tRNA^{Pyl} or to improve aminoacylation by the cognate aaRS, binding to elongation factors, and decoding in the ribosome (11,59).

This approach for generating sup-tRNAs contrasts with the more common approach of repurposing canonical tRNAs by altering the anticodon sequence, which often produces sup-tRNAs with modest PTC suppression efficiency (6,9,10). It is known that introducing mutations throughout the body and various structural segments of a sup-tRNA can improve its efficiency (5,10,60,61); however, accurately predicting which mutations will yield improvements with a given tRNA is challenging as maintaining efficient aminoacylation and decoding requires delicately balancing alteration in the target tRNA body (10). Thus, monitoring aminoacylation and translation separately may be needed during sup-tRNA development. Interestingly, our results and previous studies suggest that the sup-tRNAs' interactions with elongation factors and/or the ribosome may be more consequential for PTC translation than aminoacylation. This was evident for the *E. coli* tRNA^{Ala} and *M. mazei* tRNA^{Pyl} variants, which are effectively aminoacylated by AlaRS, yet translate UAG poorly. Inherent features in *E. coli* tRNA^{Ala} and *M. mazei* tRNA^{Pyl} mutants appear to hinder their capacity to translate PTCs, whereas *M. alvus* tRNA^{Pyl} may have evolved elements that endow it with a higher proficiency in PTC suppression.

Our results indicate that the anticodon stem-loop is a major feature of *M. alvus* tRNA^{Pyl}'s translation efficiency, supporting the notion that *M. alvus* tRNA^{Pyl} has unique features that promote the efficient translation of stop codons. However, further studies are needed to understand the role of the anticodon stem-loop in PTC suppression and if other tRNA elements play a role. Identifying and understanding the features of *M. alvus* tRNA^{Pyl} that contribute to stop codon readthrough can help design and engineer more efficient sup-tRNAs. This information may also help explain the decoding differences between canonical tRNAs and tRNA^{Pyl}. We also observed that PASS-tRNA anticodon variants showed lower suppression efficiency with UGA and UAA PTCs. The decreased activity of the anticodon variants is unlikely to be the result of lower aminoacylation by AlaRS since the PASS-tRNA mutant with UCA anticodon was aminoacylated with similar efficiency relative to the mutant with CUA anticodon (Figure 2A and B). Thus, changes in the anticodon sequence may reduce *M. alvus* PASS-tRNA decoding capacity in the ribosome. Suboptimal suppression of UAA and UGA codons by tRNA^{Pyl} in both *E. coli* and human cells has been noted previously (62,63), and

similar results have been reported for other engineered sup-tRNAs (5). Therefore, stop-codon-specific optimization may be needed during the development of future sup-tRNAs.

While growing pre-clinical data support the therapeutic promise of synthetic sup-tRNAs to treat diseases caused by nonsense and missense mutations (5,6,9,64), several aspects must be considered as this biotechnology transitions into potential clinical applications. For example, determining the translation efficiency of sup-tRNA candidates required to meet the therapeutic threshold for PTC-caused diseases will be essential. The therapeutic threshold, which indicates how much functional protein is required to reverse the effect of a pathogenic PTC, is unique to each disease and remains unknown for most PTC-related disorders (2). Nonetheless, available therapeutic threshold estimates for several diseases range from ~1% to 30% (65,66). A recent study demonstrated that the estimated threshold of 1% for mucopolysaccharidosis type I (2) can be achieved in a mouse model of the disease by a sup-tRNA that displayed a suppression efficiency of ~15% in cultured cells (6). Although an evaluation of PASS-tRNAs' PTC translation effectiveness in animals is needed, their consistent translation efficiency across different reporters in cultured cells (>30% for UAG PTCs) highlights their potential to meet the predicted therapeutic threshold for some diseases. Another consideration is tRNA dosage and delivery. Delivery of sup-tRNAs using recombinant adeno-associated virus (AAV) and lipid nanoparticle encapsulation has been shown to be effective in mice (5,6). These two approaches demonstrate that genetically encoded or *in vitro* transcribed sup-tRNAs can be administered. Delivery of *in vitro* transcribed tRNAs using lipid nanoparticles may offer more control over a desired therapeutic dosage relative to AAV delivery systems (67). Although transcription regulation can be predetermined for sup-tRNAs delivered with AAVs using promoters with a desired strength or adjusting the sup-tRNA copy number, additional cellular processes involved in tRNA processing may play a more decisive role in the cellular concentration of sup-tRNA. Ultimately, sup-tRNAs with potent suppression efficiency may be more desirable as they could lead to reduced dosages needed to achieve therapeutic efficacy and safety.

An important consideration when rescuing the synthesis of a protein from a gene with a PTC is the identity of the amino acid incorporated. PTC mutations would preferably be translated with the amino acid that restores the protein to its WT sequence. Given that disease-causing PTCs may originate from codons involving at least 10 different amino acids (67), a panel of dedicated sup-tRNAs for each amino acid would be required. However, if the amino acid residue within the protein sequence does not play a critical functional role, the corresponding PTC could be translated with another amino acid. For instance, the clinically relevant W1282X mutation in the cystic fibrosis transmembrane conductance regulator (CFTR) protein can be corrected with leucine with minimal reduction of CFTR activity (42,68). Similarly, a W401X mutation in the human iduronidase that causes mucopolysaccharidosis type I can be functionally restored by introducing tyrosine (6). For the Q1518X, E1535X, Q1785X and E1836X mutations in BRCA1, we observed different degrees of tolerance when PASS-tRNA was used to restore BRCA1 synthesis with alanine at the corresponding positions; however, all the rescued proteins displayed detectable levels of

transactivation activity. Whether the identity of the encoded amino acid is important for protein function or if restoring translation alone is sufficient will require consideration on a case-by-case basis as some amino acid substitutions will likely result in loss or reduced protein function. This is illustrated by our results with PASS-tRNA^{V2.1} and sup-tRNA^{Tyr}. These tRNAs displayed similar suppression efficiency in the dual luciferase assay, which is blind to amino acid identity. However, sup-tRNA^{Tyr} yielded lower GFP and SEAP signals, suggesting that these reporters better tolerate alanine at the PTC-encoded position. These results underscore the need for a panel of efficient sup-tRNAs with varying amino acid identity.

The translation of synthetic sup-tRNAs to the clinic also warrants further investigations due to the complex biology of tRNAs. While this and other studies demonstrate that engineered sup-tRNAs have little toxicity in cultured human cells (5,6,9), less is known about their potential long-term effects in animal models. tRNAs are engaged in many cellular interactions, including post-transcriptional modifications, aminoacylation, transport by elongation factors and the ribosome. Beyond protein synthesis, tRNAs participate in several other critical cellular processes (2,69). Infiltration of sup-tRNAs into these pathways may dysregulate cellular function. In the past decade, tRNA^{Pyl} has been introduced into different animal models for genetic code applications with no reported toxicity (17). We speculate that an advantage of using tRNA^{Pyl}-derived sup-tRNAs is their potential orthogonality to the human tRNA-interactome, which may restrict their interactions with the translation machinery, minimizing their involvement with other metabolic pathways. Additional work is needed to better understand the cellular processing of this class of artificial tRNAs.

Data availability

MS data are deposited in the ProteomeXchange Consortium via the PRIDE (70) partner repository with the dataset identifiers PXD044322 and PXD044548. RNA-seq and ribosome profiling data are available at the Gene Expression Omnibus under accession numbers GSE277128 and GSE277130, respectively.

Supplementary data

Supplementary Data are available at NAR Online.

Acknowledgements

The authors thank Sheree A. Wek, Kirk A. Staschke, Michael Holmes and Ronald C. Wek of the Department of Biochemistry and Molecular Biology, Indiana University School of Medicine, for providing advice on cell culture and ribosome profiling experiments. The MS of GFP expressed in HEK 293 was done by the Indiana University School of Medicine Centre for Proteome Analysis. Acquisition of the IUSM CPA Instrumentation used for this project was provided by the Indiana University Precision Health Initiative. We thank the quantitative proteomics analysis conducted by Drs Jeremy L. Balsbaugh and Jennifer C. Liddle of the University of Connecticut Proteomics and Metabolomics Facility, a component of the Center for Open Research Resources and Equipment at the

University of Connecticut. We also thank NIH S10 High-End Instrumentation Award 1S10-OD028445-01A1, which supported this work by providing funds to acquire the Orbitrap Eclipse Tribrid mass spectrometer housed in the University of Connecticut Proteomics & Metabolomics Facility. We are also grateful to Dr Xiang-Lei Yang and Ryan Shapiro for providing the plasmid for the recombinant purification of human AlaRS.

Funding

Indiana University School of Medicine (to J.M.T.); IUSCCC Vera Bradley and Catherine Peachy Foundation Breast Cancer Breakthrough Award (to J.M.T.); School of Medicine, University of Connecticut (to O.V.-R.); National Institutes of Health [R35GM146883 to J.-D.B and UL1TR002529]; Indiana University Precision Health Initiative; Indiana Clinical and Translational Sciences Institute; National Cancer Institute [P30CA082709]. Funding for open access charge: Indiana University School of Medicine (to J.M.T.); University of Connecticut School of Medicine (to O.V.-R.).

Conflict of interest statement

J.M.T. and O.V.-R. are co-inventors on a patent application filed jointly by Indiana University School of Medicine and the University of Connecticut School of Medicine related to the design and application of the sup-tRNAs described in this work.

References

- Keeling, K.M., Xue, X., Gunn, G. and Bedwell, D.M. (2014) Therapeutics based on stop codon readthrough. *Annu. Rev. Genomics. Hum. Genet.*, **15**, 371–394.
- Porter, J.J., Heil, C.S. and Lueck, J.D. (2021) Therapeutic promise of engineered nonsense suppressor tRNAs. *Wiley Interdiscip. Rev. RNA*, **12**, e1641.
- Dolgin, E. (2022) tRNA therapeutics burst onto startup scene. *Nat. Biotechnol.*, **40**, 283–286.
- Anastassiadis, T. and Köhrer, C. (2023) Ushering in the era of tRNA medicines. *J. Biol. Chem.*, **299**, 105246.
- Albers, S., Allen, E.C., Bharti, N., Davyt, M., Joshi, D., Perez-Garcia, C.G., Santos, L., Mukthavaram, R., Delgado-Toscano, M.A., Molina, B., et al. (2023) Engineered tRNAs suppress nonsense mutations in cells and *in vivo*. *Nature*, **618**, 842–848.
- Wang, J., Zhang, Y., Mendonca, C.A., Yukselen, O., Muneeruddin, K., Ren, L., Liang, J., Zhou, C., Xie, J., Li, J., et al. (2022) AAV-delivered suppressor tRNA overcomes a nonsense mutation in mice. *Nature*, **604**, 343–348.
- Chang, J.C., Temple, G.F., Trecartin, R.F. and Kan, Y.W. (1979) Suppression of the nonsense mutation in homozygous β^0 thalassaemia. *Nature*, **281**, 602–603.
- Temple, G.F., Dozy, A.M., Roy, K.L. and Kan, Y.W. (1982) Construction of a functional human suppressor tRNA gene: an approach to gene therapy for β -thalassaemia. *Nature*, **296**, 537–540.
- Lueck, J.D., Yoon, J.S., Perales-Puchalt, A., Mackey, A.L., Infield, D.T., Behlke, M.A., Pope, M.R., Weiner, D.B., Skach, W.R., McCray, P.B. Jr., et al. (2019) Engineered transfer RNAs for suppression of premature termination codons. *Nat. Commun.*, **10**, 822.
- Albers, S., Beckert, B., Matthies, M.C., Mandava, C.S., Schuster, R., Seuring, C., Riedner, M., Sanyal, S., Torda, A.E., Wilson, D.N., et al. (2021) Repurposing tRNAs for nonsense suppression. *Nat. Commun.*, **12**, 3850.
- Awawdeh, A., Radecki, A.A. and Vargas-Rodriguez, O. (2024) Suppressor tRNAs at the interface of genetic code expansion and medicine. *Front. Genet.*, **15**, 1420331.
- Ibba, M. and Söll, D. (2004) Aminoacyl-tRNAs: setting the limits of the genetic code. *Genes Dev.*, **18**, 731–738.
- Tharp, J.M., Ehnbo, A. and Liu, W.R. (2018) tRNA^{Pyl}: structure, function, and applications. *RNA Biol.*, **15**, 441–452.
- Chin, J.W. (2017) Expanding and reprogramming the genetic code. *Nature*, **550**, 53–60.
- Wan, W., Tharp, J.M. and Liu, W.R. (2014) Pyrrolysyl-tRNA synthetase: an ordinary enzyme but an outstanding genetic code expansion tool. *Biochim. Biophys. Acta*, **1844**, 1059–1070.
- Dumas, A., Lercher, L., Spicer, C.D. and Davis, B.G. (2015) Designing logical codon reassignment - Expanding the chemistry in biology. *Chem. Sci.*, **6**, 50–69.
- Brown, W., Liu, J. and Deiters, A. (2018) Genetic code expansion in animals. *ACS Chem. Biol.*, **13**, 2375–2386.
- Shi, N., Yang, Q., Zhang, H., Lu, J., Lin, H., Yang, X., Abulimiti, A., Cheng, J., Wang, Y., Tong, L., et al. (2022) Restoration of dystrophin expression in mice by suppressing a nonsense mutation through the incorporation of unnatural amino acids. *Nat. Biomed. Eng.*, **6**, 195–206.
- Duan, D., Goemans, N., Takeda, S.i., Mercuri, E. and Aartsma-Rus, A. (2021) Duchenne muscular dystrophy. *Nat. Rev. Dis. Primers*, **7**, 13.
- Tharp, J.M., Vargas-Rodriguez, O., Schepartz, A. and Söll, D. (2021) Genetic encoding of three distinct noncanonical amino acids using reprogrammed initiator and nonsense codons. *ACS Chem. Biol.*, **16**, 766–774.
- Jiang, H.K., Ambrose, N.L., Chung, C.Z., Wang, Y.S., Söll, D. and Tharp, J.M. (2023) Split aminoacyl-tRNA synthetases for proximity-induced stop codon suppression. *Proc. Natl Acad. Sci. U.S.A.*, **120**, e2219758120.
- Meineke, B., Heimgärtner, J., Lafranchi, L. and Elsässer, S.J. (2018) *Methanomethylophilus alvus* Mx1201 provides basis for mutual orthogonal pyrrolysyl tRNA/aminoacyl-tRNA synthetase pairs in mammalian cells. *ACS Chem. Biol.*, **13**, 3087–3096.
- Cox, J. and Mann, M. (2008) MaxQuant enables high peptide identification rates, individualized p.p.b.-range mass accuracies and proteome-wide protein quantification. *Nat. Biotechnol.*, **26**, 1367–1372.
- Vargas-Rodriguez, O., Badran, A.H., Hoffman, K.S., Chen, M., Crnković, A., Ding, Y., Krieger, J.R., Westhof, E., Söll, D. and Melnikov, S. (2021) Bacterial translation machinery for deliberate mistranslation of the genetic code. *Proc. Natl Acad. Sci. U.S.A.*, **118**, e2110797118.
- Sun, L., Gomes, A.C., He, W., Zhou, H., Wang, X., Pan, D.W., Schimmel, P., Pan, T. and Yang, X.L. (2016) Evolutionary gain of alanine mischarging to noncognate tRNAs with a G4:U69 base pair. *J. Am. Chem. Soc.*, **138**, 12948–12955.
- Kitagawa, M., Ara, T., Arifuzzaman, M., Ioka-Nakamichi, T., Inamoto, E., Toyonaga, H. and Mori, H. (2005) Complete set of ORF clones of *Escherichia coli* ASKA library (a complete set of *E. coli* K-12 ORF archive): unique resources for biological research. *DNA Res.*, **12**, 291–299.
- Schuntermann, D.B., Fischer, J.T., Bile, J., Gaier, S.A., Shelley, B.A., Awawdeh, A., Jahn, M., Hoffman, K.S., Westhof, E., Söll, D., et al. (2023) Mistranslation of the genetic code by a new family of bacterial transfer RNAs. *J. Biol. Chem.*, **299**, 104852.
- Holmes, M.J., Shah, P., Wek, R.C. and Sullivan, W.J. Jr. (2019) Simultaneous ribosome profiling of human host cells infected with *Toxoplasma gondii*. *mSphere*, **4**, e00292-19.
- McGlinchy, N.J. and Ingolia, N.T. (2017) Transcriptome-wide measurement of translation by ribosome profiling. *Methods*, **126**, 112–129.
- Weinberg, D.E., Shah, P., Eichhorn, S.W., Hussmann, J.A., Plotkin, J.B. and Bartel, D.P. (2016) Improved ribosome-footprint and mRNA measurements provide insights into dynamics and regulation of yeast translation. *Cell Rep.*, **14**, 1787–1799.

31. Wangen, J.R. and Green, R. (2020) Stop codon context influences genome-wide stimulation of termination codon readthrough by aminoglycosides. *eLife*, **9**, e52611.
32. Rodriguez, J.M., Maietta, P., Ezkurdia, I., Pietrelli, A., Wesselink, J.J., Lopez, G., Valencia, A. and Tress, M.L. (2013) APPRIS: annotation of principal and alternative splice isoforms. *Nucleic Acids Res.*, **41**, D110–D117.
33. Pujar, S., O’Leary, N.A., Farrell, C.M., Loveland, J.E., Mudge, J.M., Wallin, C., Girón, C.G., Diekhans, M., Barnes, I., Bennett, R., et al. (2018) Consensus coding sequence (CCDS) database: a standardized set of human and mouse protein-coding regions supported by expert curation. *Nucleic Acids Res.*, **46**, D221–D228.
34. Love, M.I., Huber, W. and Anders, S. (2014) Moderated estimation of fold change and dispersion for RNA-seq data with DESeq2. *Genome Biol.*, **15**, 550.
35. Abreu, R.B.V., Gomes, T.T., Nepomuceno, T.C., Li, X., Fuchshuber-Moraes, M., De Gregoriis, G., Suarez-Kurtz, G., Monteiro, A.N.A. and Carvalho, M.A. (2022) Functional restoration of *BRCA1* nonsense mutations by aminoglycoside-induced readthrough. *Front. Pharmacol.*, **13**, 935995.
36. Fernandes, V.C., Golubeva, V.A., Di Pietro, G., Shields, C., Amankwah, K., Nepomuceno, T.C., de Gregoriis, G., Abreu, R.B.V., Harro, C., Gomes, T.T., et al. (2019) Impact of amino acid substitutions at secondary structures in the BRCT domains of the tumor suppressor *BRCA1*: implications for clinical annotation. *J. Biol. Chem.*, **294**, 5980–5992.
37. Guo, L.T., Amikura, K., Jiang, H.K., Mukai, T., Fu, X., Wang, Y.S., O’Donoghue, P., Söll, D. and Tharp, J.M. (2022) Ancestral archaea expanded the genetic code with pyrrolysine. *J. Biol. Chem.*, **298**, 102521.
38. Hou, Y.M. and Schimmel, P. (1988) A simple structural feature is a major determinant of the identity of a transfer RNA. *Nature*, **333**, 140–145.
39. McClain, W.H. and Foss, K. (1988) Changing the identity of a tRNA by introducing a G-U wobble pair near the 3’ acceptor end. *Science*, **240**, 793–796.
40. Gundllapalli, S., Ambrogelly, A., Umehara, T., Li, D., Polycarpo, C. and Söll, D. (2008) Misacylation of pyrrolysine tRNA *in vitro* and *in vivo*. *FEBS Lett.*, **582**, 3353–3358.
41. Shiba, K., Ripmaster, T., Suzuki, N., Nichols, R., Plotz, P., Noda, T. and Schimmel, P. (1995) Human alanyl-tRNA synthetase: conservation in evolution of catalytic core and microhelix recognition. *Biochemistry*, **34**, 10340–10349.
42. Ko, W., Porter, J.J., Sipple, M.T., Edwards, K.M. and Lueck, J.D. (2022) Efficient suppression of endogenous CFTR nonsense mutations using anticodon-engineered transfer RNAs. *Mol. Ther. Nucleic Acids*, **28**, 685–701.
43. Borrel, G., Gaci, N., Peyret, P., O’Toole, P.W., Gribaldo, S. and Brugère, J.F. (2014) Unique characteristics of the pyrrolysine system in the 7th order of methanogens: implications for the evolution of a genetic code expansion cassette. *Archaea*, **2014**, 374146.
44. Dunkelmann, D.L., Willis, J.C.W., Beattie, A.T. and Chin, J.W. (2020) Engineered triply orthogonal pyrrolysyl-tRNA synthetase/tRNA pairs enable the genetic encoding of three distinct non-canonical amino acids. *Nat. Chem.*, **12**, 535–544.
45. Yamaguchi, A., Iraha, F., Ohtake, K. and Sakamoto, K. (2018) Pyrrolysyl-tRNA synthetase with a unique architecture enhances the availability of lysine derivatives in synthetic genetic codes. *Molecules*, **23**, 2460.
46. Aerni, H.R., Shifman, M.A., Rogulina, S., O’Donoghue, P. and Rinehart, J. (2015) Revealing the amino acid composition of proteins within an expanded genetic code. *Nucleic Acids Res.*, **43**, e8.
47. Seki, K., Galindo, J.L. and Jewett, M.C. (2022) Orthogonal tRNA expression using endogenous machinery in cell-free systems. bioRxiv doi: <https://doi.org/10.1101/2022.10.04.510903>, 05 October 2022, preprint: not peer reviewed.
48. Chen, C., Yu, G., Huang, Y., Cheng, W., Li, Y., Sun, Y., Ye, H. and Liu, T. (2022) Genetic-code-expanded cell-based therapy for treating diabetes in mice. *Nat. Chem. Biol.*, **18**, 47–55.
49. Loughran, G., Howard, M.T., Firth, A.E. and Atkins, J.F. (2017) Avoidance of reporter assay distortions from fused dual reporters. *RNA*, **23**, 1285–1289.
50. Ryter, S.W. (2022) Heme oxygenase-1: an anti-inflammatory effector in cardiovascular, lung, and related metabolic disorders. *Antioxidants*, **11**, 555.
51. Morosky, P., Comyns, C., Nunes, L.G.A., Chung, C.Z., Hoffmann, P.R., Söll, D., Vargas-Rodriguez, O. and Krahn, N. (2023) Dual incorporation of non-canonical amino acids enables production of post-translationally modified selenoproteins. *Front. Mol. Biosci.*, **10**, 1096261.
52. Brenner, S. and Beckwith, J.R. (1965) Ochre mutants, a new class of suppressible nonsense mutants. *J. Mol. Biol.*, **13**, 629–637.
53. Giegé, R. and Eriani, G. (2023) The tRNA identity landscape for aminoacylation and beyond. *Nucleic Acids Res.*, **51**, 1528–1570.
54. Li, H., Engel, C., de la Hoya, M., Peterlongo, P., Yannoukakos, D., Livraghi, L., Radice, P., Thomassen, M., Hansen, T.V.O., Gerdes, A.M., et al. (2022) Risks of breast and ovarian cancer for women harboring pathogenic missense variants in *BRCA1* and *BRCA2* compared with those harboring protein truncating variants. *Genet. Med.*, **24**, 119–129.
55. Fan, C., Xiong, H., Reynolds, N.M. and Söll, D. (2015) Rationally evolving tRNA^{Pyl} for efficient incorporation of noncanonical amino acids. *Nucleic Acids Res.*, **43**, e156.
56. Serfling, R., Lorenz, C., Eitzel, M., Schicht, G., Böttke, T., Mörl, M. and Coin, I. (2018) Designer tRNAs for efficient incorporation of non-canonical amino acids by the pyrrolysine system in mammalian cells. *Nucleic Acids Res.*, **46**, 1–10.
57. Jewel, D., Kelemen, R.E., Huang, R.L., Zhu, Z., Sundaresh, B., Cao, X., Malley, K., Huang, Z., Pasha, M., Anthony, J., et al. (2023) Virus-assisted directed evolution of enhanced suppressor tRNAs in mammalian cells. *Nat. Methods*, **20**, 95–103.
58. Niu, W., Schultz, P.G. and Guo, J. (2013) An expanded genetic code in mammalian cells with a functional quadruplet codon. *ACS Chem. Biol.*, **8**, 1640–1645.
59. Kim, Y., Cho, S., Kim, J.C. and Park, H.S. (2024) tRNA engineering strategies for genetic code expansion. *Front. Genet.*, **15**, 1373250.
60. Ogawa, A., Doi, Y. and Matsushita, N. (2011) Improvement of *in vitro*-transcribed amber suppressor tRNAs toward higher suppression efficiency in wheat germ extract. *Org. Biomol. Chem.*, **9**, 8495–8503.
61. Ogawa, A., Namba, Y. and Gakumasawa, M. (2016) Rational optimization of amber suppressor tRNAs toward efficient incorporation of a non-natural amino acid into protein in a eukaryotic wheat germ extract. *Org. Biomol. Chem.*, **14**, 2671–2678.
62. Odoi, K.A., Huang, Y., Rezenom, Y.H. and Liu, W.R. (2013) Nonsense and sense suppression abilities of original and derivative *Methanosarcina mazei* pyrrolysyl-tRNA synthetase-tRNA^{Pyl} pairs in the *Escherichia coli* BL21(DE3) cell strain. *PLoS One*, **8**, e57035.
63. Zheng, Y., Addy, P.S., Mukherjee, R. and Chatterjee, A. (2017) Defining the current scope and limitations of dual noncanonical amino acid mutagenesis in mammalian cells. *Chem. Sci.*, **8**, 7211–7217.
64. Hou, Y., Zhang, W., McGilvray, P.T., Sobczyk, M., Wang, T., Weng, S.H.S., Huff, A., Huang, S., Pena, N., Katanski, C.D., et al. (2024) Engineered mischarged transfer RNAs for correcting pathogenic missense mutations. *Mol. Ther.*, **32**, 352–371.
65. Kerem, E. (2004) Pharmacologic therapy for stop mutations: how much CFTR activity is enough? *Curr. Opin. Pulm. Med.*, **10**, 547–552.
66. Wells, D.J. (2019) What is the level of dystrophin expression required for effective therapy of Duchenne muscular dystrophy? *J. Muscle Res. Cell Motil.*, **40**, 141–150.

67. Coller, J. and Ignatova, Z. (2024) tRNA therapeutics for genetic diseases. *Nat. Rev. Drug Discov.*, **23**, 108–125.
68. Xue, X., Mutyam, V., Thakerar, A., Mobley, J., Bridges, R. J., Rowe, S. M., Keeling, K. M. and Bedwell, D. M. (2017) Identification of the amino acids inserted during suppression of CFTR nonsense mutations and determination of their functional consequences. *Hum. Mol. Genet.*, **26**, 3116–3129.
69. Schimmel, P. (2018) The emerging complexity of the tRNA world: mammalian tRNAs beyond protein synthesis. *Nat. Rev. Mol. Cell Biol.*, **19**, 45–58.
70. Perez-Riverol, Y., Bai, J., Bandla, C., García-Seisdedos, D., Hewapathirana, S., Kamatchinathan, S., Kundu, D. J., Prakash, A., Frericks-Zipper, A., Eisenacher, M., *et al.* (2022) The PRIDE database resources in 2022: a hub for mass spectrometry-based proteomics evidences. *Nucleic Acids Res.*, **50**, D543–D552.